The autism-related protein CHD8 contributes to the stemness and differentiation of mouse hematopoietic stem cells

仁田, 暁大

出版情報：九州大学, 2020, 博士（医学）, 課程博士
バージョン：

Cell Reports

Article

The autism-related protein CHD8 contributes to the stemness and differentiation of mouse hematopoietic stem cells

Graphical Abstract

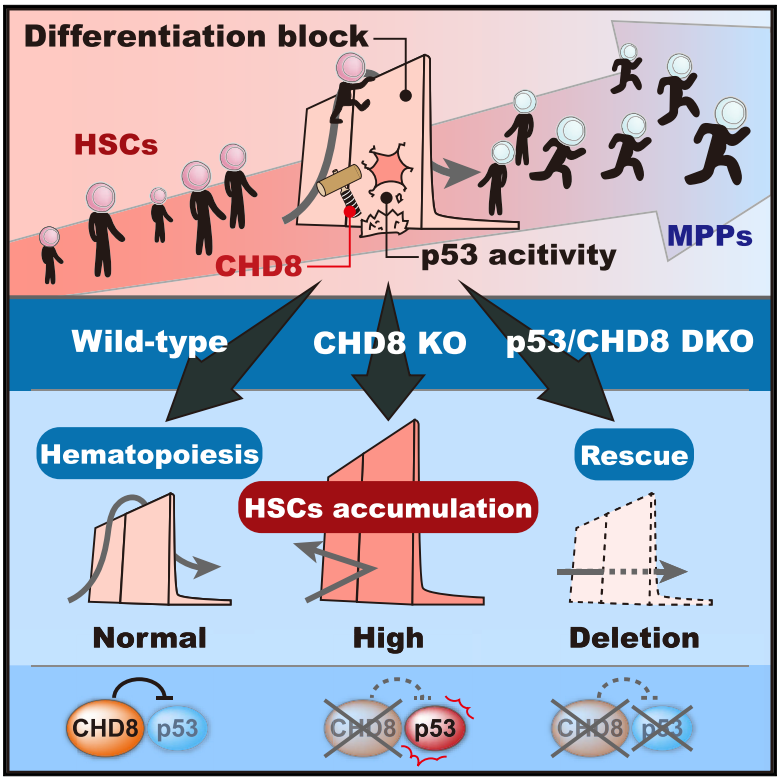

Highlights

- CHD8 is expressed at a high level in hematopoietic stem cells (HSCs)
- CHD8 loss induces cell cycle arrest, apoptosis, and a differentiation block in HSCs
- CHD8 deficiency compromises HSC stemness through activation of p53 target genes
- Additional ablation of p53 in CHD8-deficient HSCs restores stem cell function

Authors

Akihiro Nita, Yoshiharu Muto, Yuta Katayama, Akinobu Matsumoto, Masaaki Nishiyama, Keiichi I. Nakayama

Correspondence

nishiyam@staff.kanazawa-u.ac.jp (M.N.), nakayak1@bioreg.kyushu-u.ac.jp (K.I.N.)

In Brief

Nita et al. reveal that the CHD8-p53 axis plays a key role in regulation of the stemness and differentiation of hematopoietic stem cells (HSCs) *in vitro* and *in vivo*. CHD8 deficiency in HSCs results in cell cycle arrest, apoptosis, and a differentiation block, which are partially rescued by additional deletion of p53.

Nita et al., 2021, Cell Reports *34*, 108688
February 2, 2021
https://doi.org/10.1016/j.celrep.2021.108688

CellPress

Cell Reports

CellPress
OPEN ACCESS

Article

The autism-related protein CHD8 contributes to the stemness and differentiation of mouse hematopoietic stem cells

Akihiro Nita,[1] Yoshiharu Muto,[1] Yuta Katayama,[1] Akinobu Matsumoto,[1] Masaaki Nishiyama,[1,*] and Keiichi I. Nakayama[1,2,*]

[1]Department of Molecular and Cellular Biology, Medical Institute of Bioregulation, Kyushu University, 3-1-1 Maidashi, Higashi-ku, Fukuoka, Fukuoka 812-8582, Japan

[2]Lead contact

*Correspondence: nishiyam@staff.kanazawa-u.ac.jp (M.N.), nakayak1@bioreg.kyushu-u.ac.jp (K.I.N.)

https://doi.org/10.1016/j.celrep.2021.108688

SUMMARY

Chromodomain helicase DNA-binding protein 8 (CHD8) is an ATP-dependent chromatin-remodeling factor that is encoded by the most frequently mutated gene in individuals with autism spectrum disorder. CHD8 is expressed not only in neural tissues but also in many other organs; however, its functions are largely unknown. Here, we show that CHD8 is highly expressed in and maintains the stemness of hematopoietic stem cells (HSCs). Conditional deletion of *Chd8* specifically in mouse bone marrow induces cell cycle arrest, apoptosis, and a differentiation block in HSCs in association with upregulation of the expression of p53 target genes. A colony formation assay and bone marrow transplantation reveal that CHD8 deficiency also compromises the stemness of HSCs. Furthermore, additional ablation of p53 rescues the impaired stem cell function and differentiation block of CHD8-deficient HSCs. Our results thus suggest that the CHD8-p53 axis plays a key role in regulation of the stemness and differentiation of HSCs.

INTRODUCTION

Hematopoietic stem cells (HSCs) remain quiescent for long periods but enter the cell cycle to undergo self-renewal and to produce differentiated blood cells of multiple lineages (Wilson et al., 2008). This balance between self-renewal and differentiation is strictly regulated but also flexible, ensuring adequate production of blood cells under a variety of physiological conditions while also maintaining a stem cell pool (Seita and Weissman, 2010). Blood cell production must also respond efficiently to various types of hematologic stress—such as blood loss, infection, or exposure to cytotoxic agents—with this response being mediated by expansion of the hematopoietic stem and progenitor cell populations.

The HSC differentiation program is regulated by elaborate transcriptional and epigenetic mechanisms (Avgustinova and Benitah, 2016; Bröske et al., 2009; Cedar and Bergman, 2011; Cui et al., 2009). Many chromatin-modifying enzymes that contribute to the dynamics of chromatin structure and function play a role in maintenance of an appropriate size and balance of the hematologic system (Butler and Dent, 2013). In particular, chromatin remodelers, such as members of the switch/sucrose non-fermentable (SWI/SNF), imitation switch (ISWI), chromodomain helicase DNA-binding protein (CHD), and chromatin-remodeling ATPase INO80 families, have been shown to participate in the regulation of HSC fate (Prasad et al., 2015). Genome-wide interaction profiles for chromatin remodelers and nucleosomes in mouse embryonic stem cells have revealed that the remodelers regulate the fate of these cells by controlling the expression of a large number of genes (de Dieuleveult et al., 2016). The subunit composition of chromatin remodelers is altered so as to allow them to activate a set of genes that promote tissue-specific differentiation and to repress genes that reinforce self-renewal (Clapier and Cairns, 2009). Members of the CHD family of ATP-dependent chromatin remodelers contain two chromodomains, a helicase/ATPase domain and a DNA binding domain, and play an important role in stem cell maintenance and differentiation through dynamic control of chromatin structure (Micucci et al., 2015). For instance, *Chd2* nullizygous mice manifest a defect in the differentiation of HSCs into the erythroid lineage, and heterozygous mutant animals develop T cell lymphomas (Nagarajan et al., 2009). Similarly, CHD4, a component of the nucleosome remodeling and deacetylase (NuRD) complex, contributes to both the self-renewal capacity of HSCs and lineage determination. CHD4-deficient HSCs enter the cell cycle and differentiate into the erythroid lineage, but not into the myeloid or lymphoid lineages, resulting in exhaustion of HSCs and progenitors (Yoshida et al., 2008).

CHD8 was originally identified as a negative regulator of the Wnt/β-catenin signaling pathway termed Duplin (Nishiyama et al., 2012; Sakamoto et al., 2000). We showed that CHD8 suppresses the activity of the tumor suppressor protein p53 and β-catenin and thereby plays a pivotal role in cell differentiation and organogenesis (Nishiyama et al., 2009, 2012). On the other

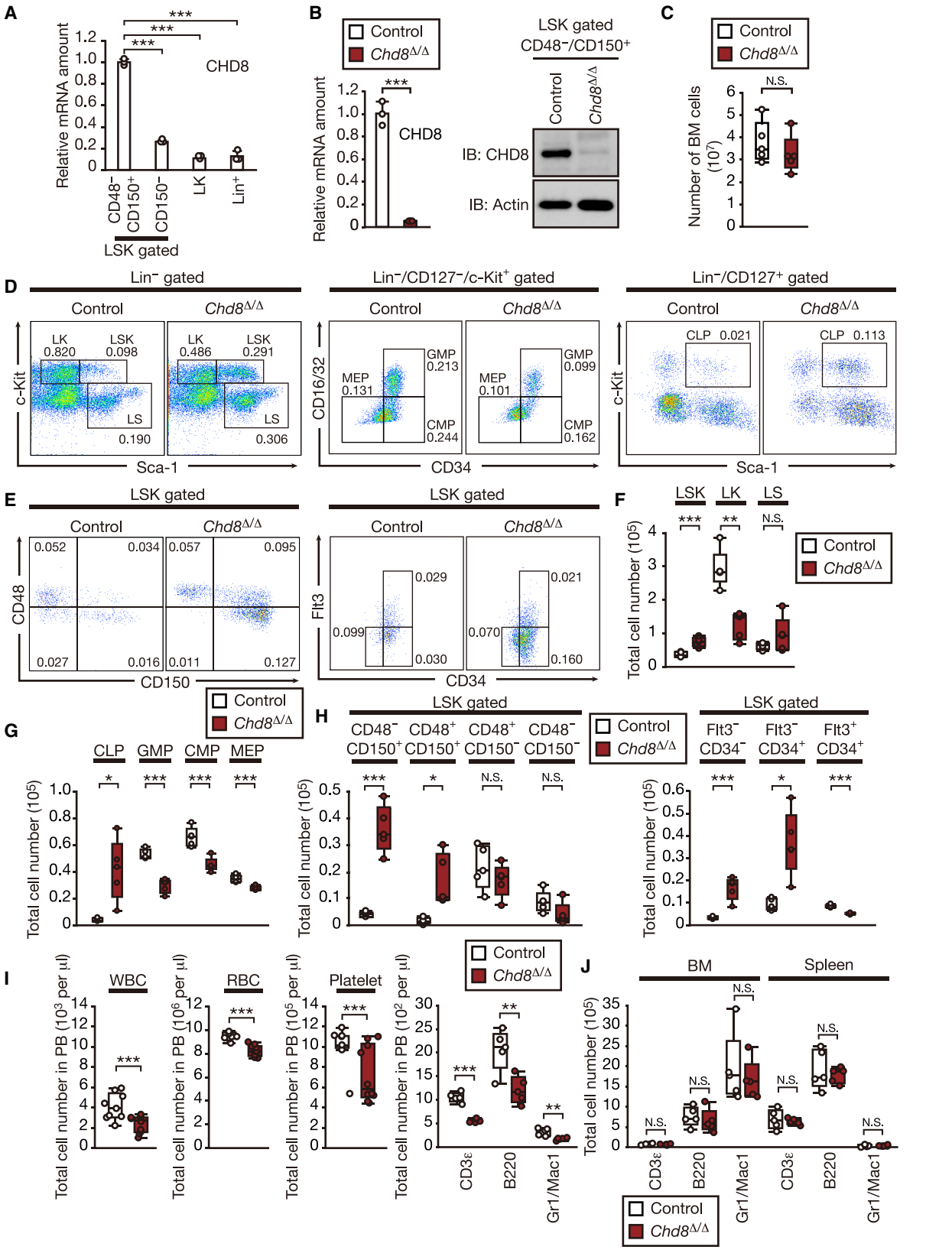

(legend on next page)

hand, *CHD8* has been shown to be the most frequently mutated gene in individuals with autism spectrum disorder (ASD) (Bernier et al., 2014; Neale et al., 2012; O'Roak et al., 2012a, 2012b; Talkowski et al., 2012). Indeed, *Chd8* haploinsufficiency in mice gives rise to ASD-like phenotypes that are associated with a delay in neuronal development (Katayama et al., 2016). Moreover, CHD8 plays an essential role not only in neuronal development but also in adipogenesis (Kita et al., 2018).

We have now established mice in which the *Chd8* gene is conditionally disrupted in the hematopoietic system in order to avoid the neonatal mortality of conventional CHD8-deficient mice. Deletion of *Chd8* resulted in an increase in HSC number and in the proportion of these cells in G_1 phase of the cell cycle as well as in impairment of their reconstitution ability after transplantation. Additional ablation of *Trp53* (which encodes p53) in the *Chd8* mutant mice largely attenuated these abnormalities. Our results thus indicate that CHD8 plays a key role in the maintenance and stemness of HSCs through regulation of p53-mediated transactivation.

RESULTS

CHD8 is essential for HSC maintenance

We examined the expression of *Chd8* in various hematopoietic cell lineages of wild-type (WT) mice by reverse transcription (RT) and real-time polymerase chain reaction (PCR) analysis. CHD8 mRNA was most abundant in the long-term HSC population (the $CD48^-CD150^+$ fraction of $Lin^-Sca\text{-}1^+c\text{-}Kit^+$ [LSK] cells, where Lin represents lineage markers), and its abundance declined in association with cell differentiation (Figure 1A). Most hematologic parameters of $Chd8^{+/-}$ mice at 12 weeks of age (at which age the mice manifest ASD-like behavior) were normal compared with $Chd8^{+/+}$ littermates, with the exception of a slight increase in the frequency of long-term HSCs ($CD48^-CD150^+$ LSK cells) in bone marrow (BM) (data not shown).

We also established mice in which *Chd8* is ablated in an inducible manner by crossing of $Chd8^{F/F}$ mice (which harbor floxed alleles of *Chd8*) with *Mx1-Cre* transgenic mice (which express Cre recombinase under the control of the *Mx1* promoter; we chose this system because mice that lack CHD8 die during embryogenesis). Intraperitoneal injection of multiple doses of poly(I:C) in the resulting offspring (*Mx1-Cre*/$Chd8^{F/F}$ mice) gives rise to the $Chd8^{\Delta/\Delta}$ genotype in HSCs. *Mx1-Cre*/$Chd8^{+/+}$ mice injected with poly(I:C) were examined as controls, excluding the possibility that the observed effects of poly(I:C) are not specific to *Chd8* deletion. The deletion efficiency for the $Chd8^F$ allele was high in hematopoietic tissue at 4 weeks after the last poly(I:C) injection, with CHD8 being almost undetectable at both mRNA and protein levels in long-term HSCs ($CD48^-CD150^+$ LSK cells; Figure 1B). As early as 4 weeks after the last poly(I:C) injection, a substantial increase in the size of the long-term HSC ($CD48^-CD150^+$ LSK) fraction as well as in the LSK, LS, common lymphoid progenitor (CLP), $CD48^+CD150^+$ LSK, $Flt3^-CD34^-$ LSK, and $Flt3^-CD34^+$ LSK populations was apparent in $Chd8^{\Delta/\Delta}$ mice compared with control littermates, whereas the total number of mononuclear cells in BM did not differ significantly between the two genotypes (Figures 1C–1H). Conversely, the size of the LK, granulocyte-monocyte progenitor (GMP), common myeloid progenitor (CMP), megakaryocyte-erythroid progenitor (MEP), and $Flt3^+CD34^+$ LSK fractions declined in CHD8-deficient mice, likely as a result of a differentiation block between HSCs and multipotent progenitors.

We further examined the effect of CHD8 ablation on the differentiation of hematopoietic cells. The $Chd8^{\Delta/\Delta}$ mice at 4 weeks after poly(I:C) injection manifested pancytopenia compared with control mice (Figure 1I), although the frequency of differentiated leukocytes ($CD3\varepsilon^+$ T cells, $B220^+$ B cells, and $Gr1^+Mac1^+$ myeloid cells) in BM or the spleen was similar for the two genotypes (Figure 1J). These results collectively suggested that CHD8 plays a key role in the regulation of hematopoiesis.

CHD8 deficiency impairs the repopulation ability of HSCs *in vitro* and *in vivo*

We next tested the colony-forming activity of LSK cells and long-term HSCs *in vitro*. The number of colonies formed by $Chd8^{\Delta/\Delta}$

Figure 1. The HSC population is increased in $Chd8^{\Delta/\Delta}$ mice

(A) RT and real-time PCR analysis of relative CHD8 mRNA abundance in Lin^+, LK, $CD150^-$ LSK, and $CD48^-CD150^+$ LSK cells isolated from BM mononuclear cells of WT mice by fluorescence-activated cell sorting (FACS). Normalized data are expressed relative to the value for $CD48^-CD150^+$ LSK cells and are means ± SD (n = 3 mice). ***$p < 0.005$ (Student's t test).

(B) RT and real-time PCR analysis of CHD8 mRNA and immunoblot (IB) analysis of CHD8 protein in long-term HSCs ($CD48^-CD150^+$ LSK cells isolated from BM of $Chd8^{\Delta/\Delta}$ or control mice at 4 weeks after the last poly(I:C) injection). Smooth muscle actin was examined as a loading control for immunoblot analysis. The mRNA data are means ± SD (n = 3 mice). ***$p < 0.005$ (Student's t test).

(C) Number of BM cells in $Chd8^{\Delta/\Delta}$ or control mice at 4 weeks after the last poly(I:C) injection. Data are presented as box-and-whisker plots (n = 5 mice). N.S., not significant (Student's t test).

(D and E) Representative flow cytometric analysis of Lin^- cells, $Lin^-CD127^-c\text{-}Kit^+$ cells, and Lin^-CD127^+ cells (D) as well as of LSK cells (E) isolated from BM mononuclear cells of $Chd8^{\Delta/\Delta}$ or control mice at 4 weeks after the last poly(I:C) injection.

(F and G) Total cell number for LSK, LK, and LS cells (F) as well as for CLP, GMP, CMP, and MEP cells (G) among BM mononuclear cells of $Chd8^{\Delta/\Delta}$ or control mice at 4 weeks after the last poly(I:C) injection. Data are presented as box-and-whisker plots (n = 5 mice). *$p < 0.05$; **$p < 0.01$; ***$p < 0.005$; N.S. (Student's t test).

(H) Total cell number for $CD48^-CD150^+$ LSK, $CD48^+CD150^+$ LSK, $CD48^+CD150^-$ LSK, and $CD48^-CD150^-$ LSK cells as well as for $Flt3^-CD34^-$ LSK, $Flt3^-CD34^+$ LSK, and $Flt3^+CD34^+$ LSK cells among BM mononuclear cells of $Chd8^{\Delta/\Delta}$ or control mice at 4 weeks after the last poly(I:C) injection. Data are presented as box-and-whisker plots (n = 5 mice). *$p < 0.05$; ***$p < 0.005$; N.S. (Student's t test).

(I) Total cell number for white blood cells (WBCs), red blood cells (RBCs), platelets, $CD3\varepsilon^+$ T cells, $B220^+$ B cells, and $Gr1^+Mac1^+$ myeloid cells in peripheral blood (PB) of $Chd8^{\Delta/\Delta}$ or control mice at 4 weeks after the last poly(I:C) injection. Data are presented as box-and-whisker plots (n = 10 mice). **$p < 0.01$; ***$p < 0.005$ (Student's t test).

(J) Total cell number for $CD3\varepsilon^+$ T cells, $B220^+$ B cells, and $Gr1^+Mac1^+$ myeloid cells in BM and the spleen of $Chd8^{\Delta/\Delta}$ or control mice at 4 weeks after the last poly(I:C) injection. Data are presented as box-and-whisker plots (n = 5 mice). N.S. (Student's t test).

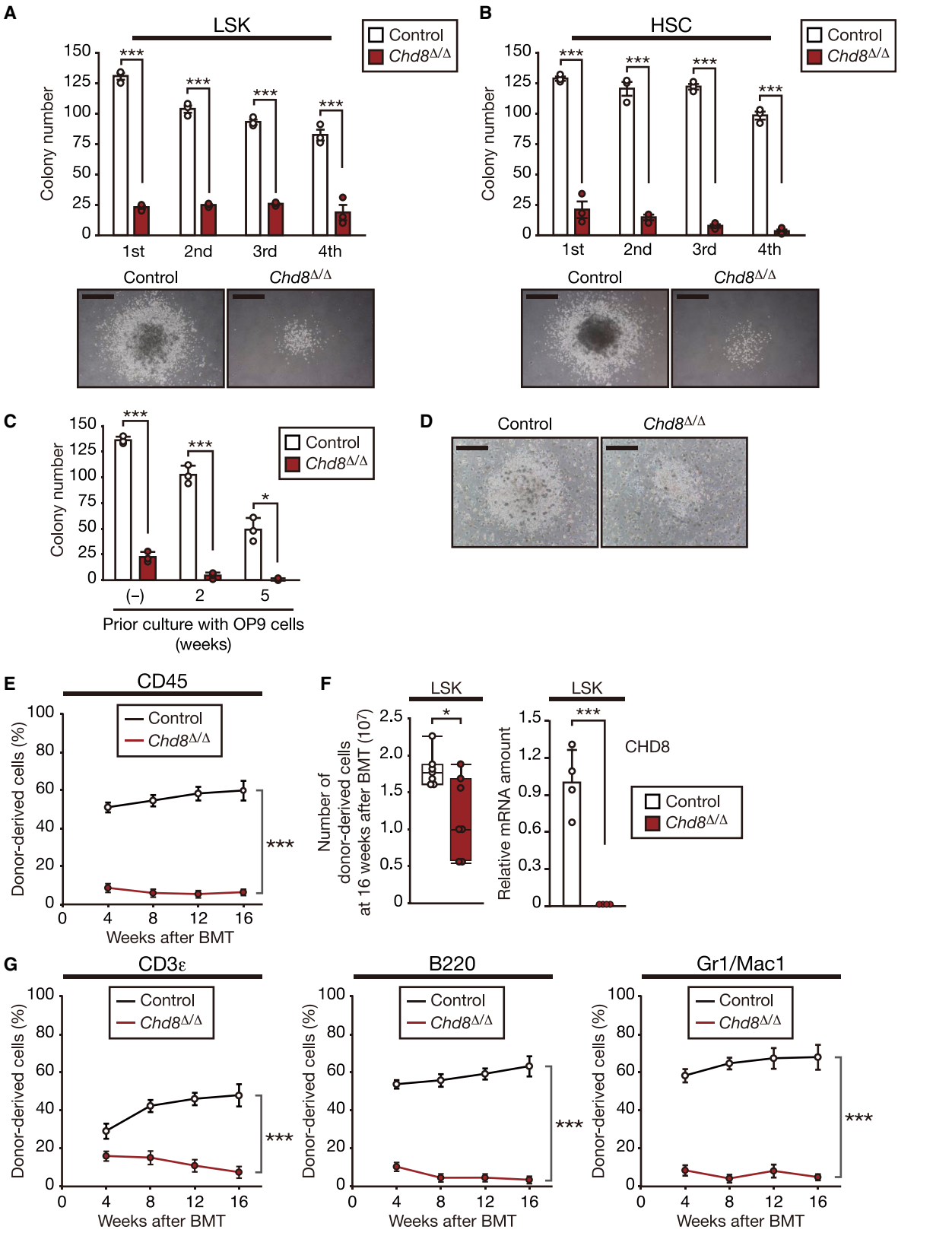

(legend on next page)

LSK cells or long-term HSCs was significantly reduced, and the size of individual colonies formed by these cells was markedly smaller compared with those formed by the corresponding cells of control mice (Figures 2A and 2B). LSK cells were also subjected to long-term culture on a layer of OP9 stromal cells, with the number of colony-forming cells arising at 2 or 5 weeks after the onset of culture reflecting the function of hematopoietic progenitor or stem cells, respectively. The number of colonies derived from *Chd8*$^{\Delta/\Delta}$ LSK cells after coculture for 2 or 5 weeks was significantly reduced compared with that derived from control LSK cells (Figures 2C and 2D). Together, these results suggested that CHD8 deficiency impairs the ability of HSCs to undergo self-renewal and differentiation.

Given that CHD8 deficiency compromised the stemness of HSCs *in vitro*, we examined whether a similar phenotype was apparent *in vivo* by BM transplantation. A competitive reconstitution assay was performed in which BM cells (4×10^5) from *Chd8*$^{\Delta/\Delta}$ or control mice (CD45.2) competed with an equal number of BM cells from C57BL/6 heterozygous congenic mice (CD45.1/CD45.2) to reconstitute the hematopoietic compartment of irradiated C57BL/6 congenic mouse recipients (CD45.1). Flow cytometric analysis of peripheral blood (PB) of the recipients revealed that the repopulating capacity of *Chd8*$^{\Delta/\Delta}$ BM cells was markedly compromised from 4 weeks after BM transplantation compared with that of control BM cells (Figures 2E and 2G). However, *Chd8*$^{\Delta/\Delta}$ LSK cells were present in BM at 16 weeks after BM transfer (Figure 2F), suggesting that the development of *Chd8*$^{\Delta/\Delta}$ LSK cells was impaired as a result of a differentiation block. Collectively, these results indicated that CHD8 is essential for maintenance of stem cell capacity in HSCs.

Chd8$^{\Delta/\Delta}$ HSCs undergo p53-dependent cell cycle arrest and apoptosis

To investigate the mechanism by which CHD8 ablation impairs HSC function, we examined gene expression profiles of control and *Chd8*$^{\Delta/\Delta}$ long-term HSCs. RNA sequencing analysis identified 2,582 differentially expressed genes (1,531 upregulated and 1,051 downregulated genes) in *Chd8*$^{\Delta/\Delta}$ HSCs compared with control cells at 4 weeks after the last poly(I:C) injection (Figure 3A; Table S1). The expression level of the gene for p21 (*Cdkn1a*), a p53 target gene, was significantly increased in *Chd8*$^{\Delta/\Delta}$ HSCs. Gene set enrichment analysis (GSEA) revealed that the p53 pathway was substantially activated in *Chd8*$^{\Delta/\Delta}$ HSCs, whereas target genes of Wnt/β-catenin signaling were not affected by CHD8 ablation (Figures 3B and 3C). Increased expression of p53 target genes, such as those encoding p21, Puma, Aen, and Apaf1 in *Chd8*$^{\Delta/\Delta}$ HSCs, was confirmed by RT and real-time PCR analysis, although the expression of *Trp53* itself did not differ between *Chd8*$^{\Delta/\Delta}$ and control HSCs (Figure 3D).

We next examined the binding of CHD8 to p53 target genes in HSCs by chromatin immunoprecipitation and quantitative PCR (ChIP-qPCR) analysis. Peaks of p53 binding were previously detected around the transcription start sites (TSSs) of the p21 and Puma genes in HPC7 cells (Wilson et al., 2016). We therefore assessed whether CHD8 binds to the TSS-neighboring regions of these genes in BM cells from WT mice (Figure 3E). We found that CHD8 bound to the TSS regions of both genes. Furthermore, similar ChIP-qPCR analysis of long-term HSCs also revealed CHD8 binding to the TSS regions of the p21 and Puma genes (Figure 3F). These results thus indicated that CHD8 negatively regulates p53 function in HSCs, consistent with its previously described role during embryonic development in mice (Nishiyama et al., 2009).

We next evaluated the cell cycle kinetics of *Chd8*$^{\Delta/\Delta}$ LSK cells and long-term HSCs by intracellular staining of the proliferation marker Ki-67 and analysis of DNA ploidy by staining with Hoechst 33342. Consistent with the increased expression of p53 target genes, the proportion of LSK cells or long-term HSCs in G_1 phase of the cell cycle (Ki-67$^+$Hoechst 33342^{low} fraction) was markedly increased for *Chd8*$^{\Delta/\Delta}$ cells compared with control cells, whereas that in G_0 phase (Ki-67$^-$Hoechst 33342^{low} fraction) was reduced (Figures 4A–4C). We also performed a 5-bromo-2′-deoxyuridine (BrdU) incorporation assay for LSK cells to assess cell cycle status, and we found that the incorporation of BrdU in *Chd8*$^{\Delta/\Delta}$ LSK cells was significantly reduced compared with that in control LSK cells (Figure 4D). These results suggested that the G_1-S transition of *Chd8*$^{\Delta/\Delta}$ LSK cells and long-term HSCs is blocked, presumably as a result of upregulation of the p53 pathway. Furthermore, RNA sequencing analysis showed that the expression of genes specific to G_1 phase was highly upregulated in *Chd8*$^{\Delta/\Delta}$ long-term HSCs, whereas that of genes specific to G_0 phase was downregulated (Figure 4E). In addition, the expression of *Ccnb1* and *Ccnb2*, both of which are expressed during S-G_2-M phases, was upregulated in the *Chd8*$^{\Delta/\Delta}$ HSCs. CHD8-deficient HSCs may therefore have escaped from G_0 phase and become subject to G_1 arrest, with a slight increase in the number of HSCs in S-G_2-M phases also being apparent. The frequency of annexin V$^+$ apoptotic cells was also increased among *Chd8*$^{\Delta/\Delta}$ HSCs compared with control HSCs at 4 weeks after the last

Figure 2. Depletion of CHD8 impairs the repopulation ability of HSCs *in vitro* and *in vivo*

(A and B) Serial replating assay of colony formation by *Chd8*$^{\Delta/\Delta}$ or control LSK cells (A) and long-term HSCs (B). Representative colonies (scale bars, 0.5 mm) and quantitative data (means ± SD) from three independent experiments are shown. ***$p < 0.005$ (Student's t test).

(C) *In vitro* colony-formation capacity of *Chd8*$^{\Delta/\Delta}$ or control LSK cells with or without prior coculture with OP9 cells for 2 or 5 weeks. Data are means ± SD (n = 3 independent experiments). *$p < 0.05$; ***$p < 0.005$ (Student's t test).

(D) Representative colonies from an experiment as in (C). Scale bars, 0.5 mm.

(E) Donor BM cells (4×10^5) from *Chd8*$^{\Delta/\Delta}$ or control mice were transplanted together with an equal number of competitor BM cells into lethally irradiated recipient mice (n = 7 mice). The percentage of donor-derived cells among CD45$^+$ cells in PB was determined at the indicated times after BM transplantation (BMT). Data are means ± SD. ***$p < 0.005$ (Student's t test).

(F) The number of donor-derived LSK cells in BM (n = 7 recipients) and relative CHD8 mRNA amount in total LSK cells (n = 4 recipients) at 16 weeks after BM transfer as in (E). Data are presented as box-and-whisker plots and as means ± SD, respectively. *$p < 0.05$; ***$p < 0.005$ (Student's t test).

(G) The percentage of donor-derived cells among CD3ε$^+$ T cells, B220$^+$ B cells, and Gr1$^+$Mac1$^+$ myeloid cells in PB was determined at the indicated times after BM transplantation (n = 7 recipients) as in (E). Data are means ± SD. ***$p < 0.005$ (Student's t test).

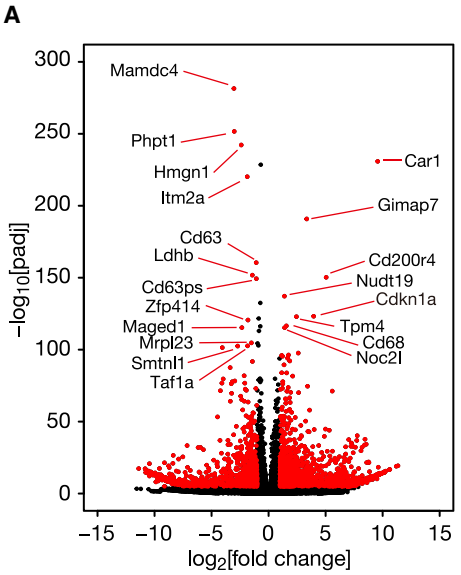

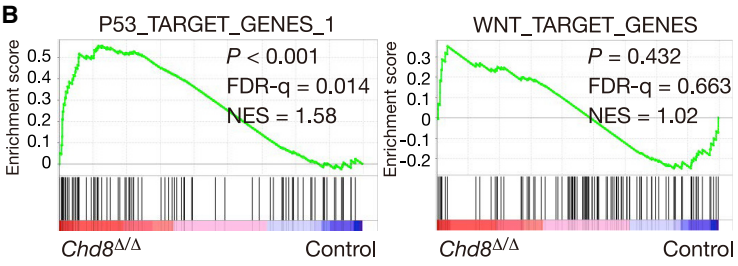

C

Gene set	NES	NOM *P* value	FDR *q* value
P53_TARGET_GENES_1	1.58	< 0.001	0.014
P53_TARGET_GENES_2	1.55	0.002	0.015
P53_TARGET_GENES_3	1.38	0.072	0.193
WNT_TARGET_GENES	1.02	0.432	0.663
KEGG_WNT_SIGNALING_PATHWAY	0.91	0.685	0.765
KENNY_CTNNB1_TARGETS_UP	0.89	0.661	0.679

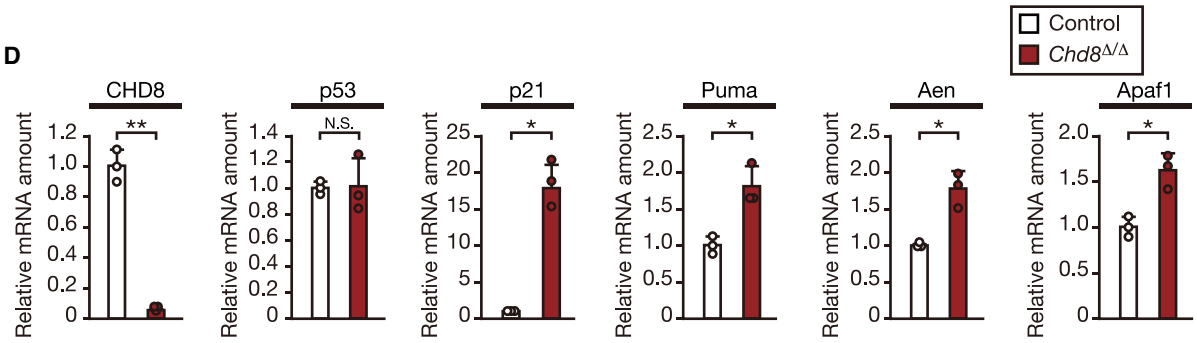

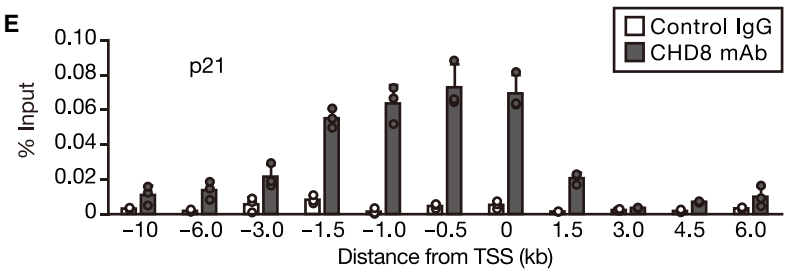

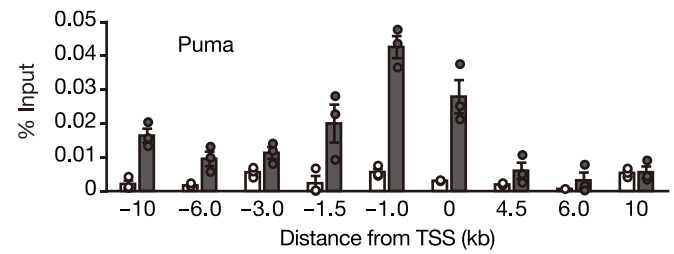

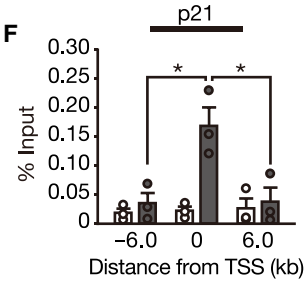

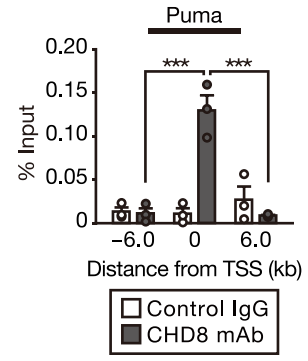

(legend on next page)

poly(I:C) injection (Figure 4F). To exclude the possibility that *Chd8* deletion induces DNA damage and thereby activates the p53 pathway, we performed immunofluorescence analysis with antibodies to γ-H2AX in the mutant HSCs (Figure 4G). The number of γ-H2AX foci in $Chd8^{\Delta/\Delta}$ HSCs was similar to that in control cells, suggesting that *Chd8* deletion did not give rise to DNA damage that was in turn responsible for p53 activation. Together, these findings suggested that increased activity of p53 as a result of CHD8 deficiency induces cell cycle arrest and apoptosis in HSCs, likely accounting for the impaired BM reconstitution by $Chd8^{\Delta/\Delta}$ HSCs. Despite such cell cycle arrest and increased apoptosis, however, the size of the long-term HSC population was paradoxically increased in $Chd8^{\Delta/\Delta}$ mice, reminiscent of the phenotype of Wip1-deficient mice, which manifest an increased HSC population as a result of a differentiation block mediated by hyperactivated p53 (Chen et al., 2015). The accumulation of long-term HSCs in $Chd8^{\Delta/\Delta}$ mice is thus likely attributable to a differentiation block induced by p53 hyperactivity in these cells.

Additional deletion of *Trp53* rescues impaired stemness of $Chd8^{\Delta/\Delta}$ HSCs

Given that CHD8 is a key negative regulator of p53 activity, we examined the effects of additional deletion of *Trp53* in *Mx1-Cre*/$Chd8^{F/F}$ mice. At 4 weeks after the last poly(I:C) injection, the substantial increases in the size of the long-term HSC ($CD48^{-}CD150^{+}$ LSK cell) fraction as well as in that of the CLP and $Flt3^{-}CD34^{-}$ LSK populations apparent in $Chd8^{\Delta/\Delta}$ mice were partially reversed in $Trp53^{-/-}/Chd8^{\Delta/\Delta}$ mice (Figure 5). On the other hand, the size of the LSK, LK, CMP, MEP, $CD48^{+}CD150^{-}$ LSK, $CD48^{-}CD150^{-}$ LSK, and $Flt3^{+}CD34^{+}$ LSK populations was increased in $Trp53^{-/-}/Chd8^{\Delta/\Delta}$ mice compared with $Chd8^{\Delta/\Delta}$ mice. These results suggested that HSCs that had accumulated in BM and lost stem cell function as a result of *Chd8* deletion were able to overcome their differentiation block and differentiate into downstream functional progenitor cells in response to additional deletion of *Trp53*. Our RNA sequencing data for cell-cycle-related genes also revealed that CHD8-deficient HSCs may have exited from G_0 phase, with additional deletion of *Trp53* in long-term HSCs possibly resulting in a temporary overproduction of differentiated cells and increase in the size of these fractions. On the other hand, the size of the GMP population was further reduced by *Trp53* deletion in $Chd8^{\Delta/\Delta}$ mice, suggesting that another mechanism that is independent of the CHD8-p53 system might be responsible for control of the size of the GMP fraction.

We next examined the effect of additional *Trp53* deletion on the impaired stemness of $Chd8^{\Delta/\Delta}$ HSCs *in vitro* and *in vivo*. The number of colonies formed by $Trp53^{-/-}/Chd8^{\Delta/\Delta}$ LSK cells or long-term HSCs *in vitro* was significantly increased compared with that formed by the corresponding cells of $Chd8^{\Delta/\Delta}$ mice (Figures 6A and 6C). The size of individual colonies formed by $Trp53^{-/-}/Chd8^{\Delta/\Delta}$ LSK cells or long-term HSCs was similar to that for corresponding control and $Trp53^{-/-}/Chd8^{F/F}$ cells (Figures 6B and 6D). Furthermore, we transplanted BM cells from control (*Mx1-Cre*), $Trp53^{-/-}/Chd8^{F/F}$, *Mx1-Cre*/$Chd8^{F/F}$, or $Trp53^{-/-}$/*Mx1-Cre*/$Chd8^{F/F}$ mice not treated with poly(I:C) into lethally irradiated recipients together with competitor cells so as to exclude the possibility of homing defects or cell death before BM transfer. 4 weeks after BM transfer, we confirmed that control and *Mx1-Cre*/$Chd8^{F/F}$ donor cells had reconstituted BM in the recipient mice to a similar extent, and we then injected the recipient mice with poly(I:C) (Muto et al., 2017). The number of cells derived from *Mx1-Cre*/$Chd8^{F/F}$ mice declined rapidly after poly(I:C) injection (Figures 6E and 6F), suggesting that hematopoietic reconstitution capacity after homing and engraftment was impaired in $Chd8^{\Delta/\Delta}$ HSCs. On the other hand, $Trp53^{-/-}/Chd8^{F/F}$ and $Trp53^{-/-}$/*Mx1-Cre*/$Chd8^{F/F}$ donor cells reconstituted BM of recipient mice to a greater extent than did control cells, consistent with previous observations for p53-deficient cells (TeKippe et al., 2003). The number of cells derived from $Trp53^{-/-}/Chd8^{F/F}$ or $Trp53^{-/-}$/*Mx1-Cre*/$Chd8^{F/F}$ mice did not decline after poly(I:C) injection, unlike that of *Mx1-Cre*/$Chd8^{F/F}$ cells (Figures 6E and 6F).

We also evaluated the survival rate of control, $Trp53^{-/-}/Chd8^{F/F}$, *Mx1-Cre*/$Chd8^{F/F}$, and $Trp53^{-/-}$/*Mx1-Cre*/$Chd8^{F/F}$ mice injected with 5-fluorouracil (5-FU) at 4 weeks after the last poly(I:C) injection in order to eliminate differentiated hematopoietic cells and induce the activation and proliferation of HSCs. The survival rate of the $Chd8^{\Delta/\Delta}$ mice began to decline rapidly at ~10 days after 5-FU injection, whereas no control mice and most $Trp53^{-/-}/Chd8^{\Delta/\Delta}$ mice survived for up to 90 days (Figure 6G), indicating that a defect in stress-induced hematopoiesis in CHD8-deficient HSCs is rescued by the additional deletion of *Trp53*. Moreover, to exclude the possibility that the 5-FU-induced death of $Chd8^{\Delta/\Delta}$ mice was due to toxic effects of 5-FU on other tissues (Miyamoto et al., 2007), we repopulated the hematopoietic system of lethally irradiated recipients with

Figure 3. Abnormal activation of the p53 pathway in CHD8-depleted HSCs

(A) Volcano plot of differentially expressed genes in long-term HSCs isolated from $Chd8^{\Delta/\Delta}$ or control mice at 4 weeks after the last poly(I:C) injection. The 1,531 upregulated and 1,051 downregulated genes in $Chd8^{\Delta/\Delta}$ HSCs with an adjusted $p < 0.00001$ and $\log_2$[fold change] of >1 or <−1 are shown as red dots, and the names of the 20 genes with the largest $-\log_{10}$[padj] values among these genes are indicated.

(B) GSEA plots for lists of genes related to the p53 pathway or Wnt/β-catenin signaling pathway constructed from the RNA sequencing data for $Chd8^{\Delta/\Delta}$ and control HSCs as in (A). FDR, false discovery rate; NES, normalized enrichment score.

(C) Results of GSEA for several p53 target gene and Wnt/β-catenin signaling pathway gene sets. NOM, nominal.

(D) RT and real-time PCR analysis of CHD8, p53, and p53 target gene mRNA abundance in long-term HSCs isolated from BM of $Chd8^{\Delta/\Delta}$ or control mice at 4 weeks after the last poly(I:C) injection. Normalized data are expressed relative to the value for control cells. Data are means ± SD (n = 3 mice). *$p < 0.05$; **$p < 0.01$; N.S. (Student's t test).

(E and F) ChIP-qPCR analysis of the TSS regions of the p21 and Puma genes in BM cells (E) and long-term HSCs (F) of WT mice. The analysis was performed with a rat monoclonal antibody (mAb) to CHD8 or with control immunoglobulin G (IgG). Data are means ± SD (n = 3 independent experiments). *$p < 0.05$; ***$p < 0.005$ (Student's t test).

See also Table S1.

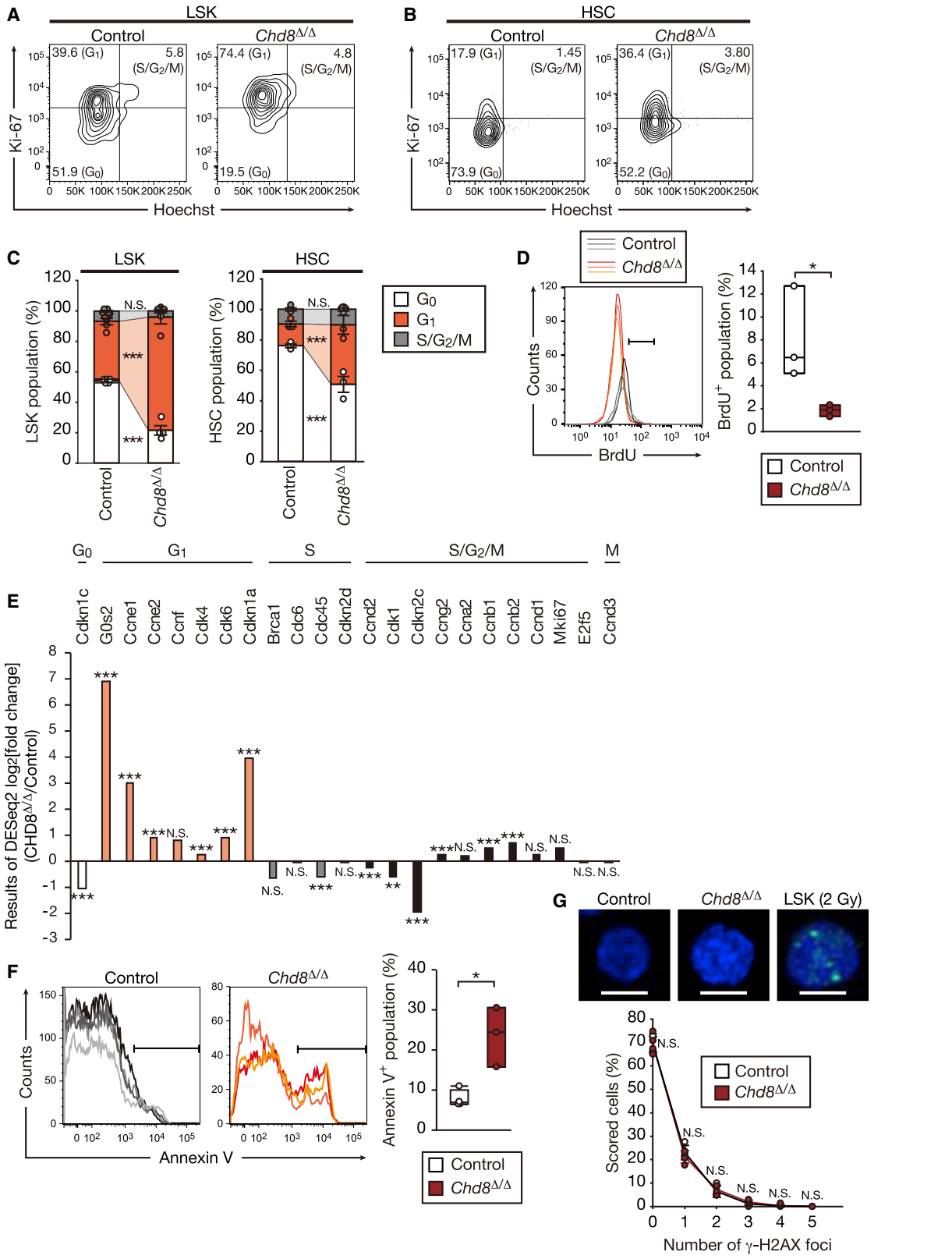

(legend on next page)

BM cells from control, *Mx1-Cre/Chd8*$^{F/F}$, *Trp53*$^{-/-}$*/Chd8*$^{F/F}$, or *Trp53*$^{-/-}$*/Mx1-Cre/Chd8*$^{F/F}$ mice that had not been treated with poly(I:C). 4 weeks after BM transfer, we confirmed that donor cells had reconstituted BM of the recipient mice and then injected the animals first with poly(I:C) and, 4 weeks after the last poly(I:C) injection, with 5-FU. The survival rate of the *Chd8*$^{\Delta/\Delta}$ mice began to decline rapidly at ~2 weeks after 5-FU injection, whereas about one-third of *Trp53*$^{-/-}$*/Chd8*$^{\Delta/\Delta}$ mice survived for at least 90 days (Figure 6H), indicating that impairment of stress-induced hematopoiesis was responsible for the 5-FU-induced death of *Chd8*$^{\Delta/\Delta}$ mice and that this defect was rescued by the additional deletion of *Trp53*. These results thus suggested that the stemness of CHD8-deficient HSCs both *in vitro* and *in vivo* is partially restored by the additional ablation of *Trp53*.

Transcriptomic landscape of *Chd8*$^{\Delta/\Delta}$ and *Trp53*$^{-/-}$ HSCs

Finally, to characterize further the partial rescue of stemness capacity by additional deletion of *Trp53* in CHD8-deficient HSCs, we examined gene expression profiles of control, *Trp53*$^{-/-}$, *Chd8*$^{\Delta/\Delta}$, and *Trp53*$^{-/-}$*/Chd8*$^{\Delta/\Delta}$ HSCs at 4 weeks after the last poly(I:C) injection. RNA sequencing analysis identified 142 (*Trp53*$^{-/-}$), 303 (*Chd8*$^{\Delta/\Delta}$), and 306 (*Trp53*$^{-/-}$*/Chd8*$^{\Delta/\Delta}$) differentially expressed genes, including 98, 160, and 102 upregulated genes and 44, 143, and 204 downregulated genes, respectively (Figure 7A; Tables S2–S4). GSEA revealed that the activation of the p53 pathway apparent in *Chd8*$^{\Delta/\Delta}$ HSCs was indeed attenuated by the additional deletion of *Trp53* in these cells (Figures 7B and 7C). GSEA also showed no significant enrichment for the expression of genes defined in HSC- or stem-cell-related gene sets (IVANOVA_HEMATOPOIESIS_STEM_CELL, CONRAD_STEM_CELL, and BYSTRYKH_HEMATOPOIESIS_STEM_CELL_QTL_CIS) between control and either *Trp53*$^{-/-}$, *Chd8*$^{\Delta/\Delta}$, or *Trp53*$^{-/-}$*/Chd8*$^{\Delta/\Delta}$ HSCs (Figures 7D and 7E), and the abundance of mRNAs for p53 target genes was similar for *Trp53*$^{-/-}$*/Chd8*$^{F/F}$ and *Trp53*$^{-/-}$*/Chd8*$^{\Delta/\Delta}$ HSCs (Figure 7F). These results suggested that stem cell identity was not significantly affected by the loss of CHD8 or p53, despite the marked impairment of stem cell function in *Chd8*$^{\Delta/\Delta}$ HSCs revealed by loss of the ability to mediate reconstruction of the hematopoietic system after BM transplantation *in vivo* as well as by the defective self-renewal and differentiation abilities detected by colony-formation assays *in vitro*.

DISCUSSION

We have shown here that CHD8 is highly expressed in HSCs in the steady state and plays an essential role in maintenance of their self-renewal and pluripotency by suppressing p53 activity. Whereas *Chd8*$^{+/-}$ mice manifested a slight increase in the size of the HSC population but no other overt abnormalities in the hematopoietic system, the stemness and differentiation of *Chd8*$^{\Delta/\Delta}$ HSCs were markedly impaired, resulting in a decrease in the number of descendant cells and consequent pancytopenia. The *Chd8*$^{\Delta/\Delta}$ mice died within 2 weeks after 5-FU administration. These features of *Chd8*$^{\Delta/\Delta}$ HSCs are likely attributable to aberrant activation of p53, whose function is normally suppressed by CHD8. In general, p53 serves to restrain the cell cycle and to induce apoptosis, and we indeed detected cell cycle arrest and apoptosis induction in *Chd8*$^{\Delta/\Delta}$ HSCs in association with upregulation of the expression of p53 target genes. These defects in regulation of the cell cycle and apoptosis due to aberrant p53 activation likely account for the loss of stemness in *Chd8*$^{\Delta/\Delta}$ HSCs, with this notion receiving further support by our observations that additional ablation of p53 greatly ameliorated most phenotypes of *Chd8*$^{\Delta/\Delta}$ HSCs. This situation is thus similar to the previous finding that *Trp53* deletion partially rescued the impaired embryonic development of CHD8-null mice (Nishiyama et al., 2009).

The p53 protein plays a key role in the function of long-term tissue stem cells by maintaining quiescence in the steady state (Liu et al., 2009a; Pant et al., 2012; Solozobova and Blattner, 2011; Yamashita et al., 2016). Loss of p53 in HSCs results in an increase in their proliferation but does not enhance their stem cell function (Chen et al., 2008). The highly proliferative p53-deficient HSCs are impaired in their repopulation capacity compared to their WT counterparts (Akala et al., 2008; Chen et al., 2008; Liu et al., 2009a; TeKippe et al., 2003), suggesting that the absence of p53 compromises the functional fitness of HSCs. On the other hand, total BM cells from p53-deficient mice outgrow WT cells in competitive BM transplantation assays, indicating that either progenitor cells or external factors originating in BM modulate HSC function (Pant et al., 2012). Excessive activation of p53 is also detrimental to the hematopoietic system (Chen et al., 2008).

Figure 4. p53-dependent cell cycle arrest and apoptosis in CHD8-null HSCs

(A) Cell cycle status of LSK cells isolated from BM of *Chd8*$^{\Delta/\Delta}$ (n = 4) or control (n = 5) mice at 4 weeks after the last poly(I:C) injection and stained with antibodies to Ki-67 and Hoechst 33342 for determination of the percentage of cells in G_0, G_1, and S-G_2-M phases. Representative flow cytometric traces are shown.

(B) Cell cycle status of long-term HSCs isolated from BM of *Chd8*$^{\Delta/\Delta}$ (n = 3) or control (n = 3) mice as in (A).

(C) The percentage of LSK cells or long-term HSCs in G_0, G_1, and S-G_2-M phases determined as in (A) and (B). Data are presented as stacked bars showing mean ± SD values. ***$p < 0.005$; N.S. (Student's t test).

(D) Flow cytometric traces and quantitation of BrdU incorporation in LSK cells isolated from BM of *Chd8*$^{\Delta/\Delta}$ or control mice at 4 weeks after the last poly(I:C) injection. Quantitative data are presented as box-and-whisker plots (n = 3 mice). *$p < 0.05$ (Student's t test).

(E) RNA sequencing data for differentially expressed cell-cycle-related genes in *Chd8*$^{\Delta/\Delta}$ versus control HSCs at 4 weeks after the last poly(I:C) injection. **$p < 0.01$; ***$p < 0.005$; N.S. (adjusted p value).

(F) The percentage of apoptotic (annexin V$^+$) cells was determined for long-term HSCs isolated from BM of *Chd8*$^{\Delta/\Delta}$ or control mice at 4 weeks after the last poly(I:C) injection. Data are presented as box-and-whisker plots (n = 3 mice). *$p < 0.05$ (Student's t test). Representative flow cytometric traces are also shown.

(G) Immunofluorescence analysis of γ-H2AX (green fluorescence) in long-term HSCs isolated from BM of *Chd8*$^{\Delta/\Delta}$ or control mice at 4 weeks after the last poly(I:C) injection as well as in LSK cells isolated from WT mice and exposed to 2 Gy of ionizing radiation (positive control). Nuclei were stained with 4′,6-diamidino-2-phenylindole (DAPI) (blue fluorescence). Scale bars, 10 μm. The percentages of scored HSCs containing the indicated numbers of γ-H2AX foci are presented as means ± SD (n = 3 mice). N.S. (Student's t test).

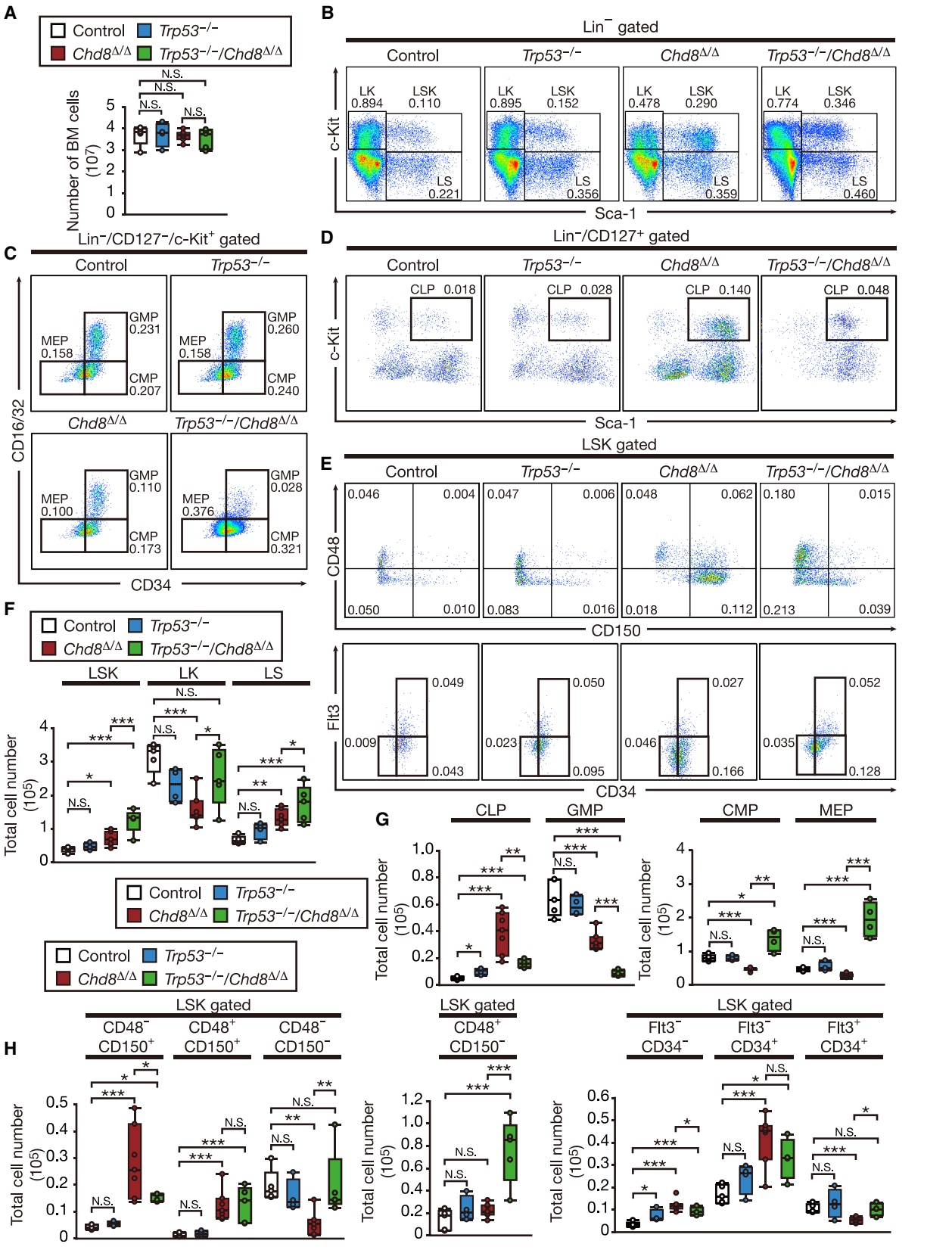

(legend on next page)

It therefore seems important that the amount and function of p53 be strictly regulated, with disruption of such regulatory mechanisms giving rise to impairment of blood cell supply. One such control system is repression of p53 target genes by CHD8. The key role of p53 in regulation of HSC quiescence is also manifest by its promotion of the enhanced quiescence characteristic of HSCs that lack the mouse embryonic fibroblast (MEF)/E74 like ETS transcription factor 4 (ELF4) transcription factor (Liu et al., 2009b). Additional ablation of p53 in MEF/ELF4-deficient HSCs thus accelerated re-entry of the quiescent cells into the cell cycle, with this effect being thought to be independent of p21 (Liu et al., 2009b). Given that p53 negatively regulates self-renewal of HSCs, CHD8 likely plays a key role as a functional negative regulator of p53 in these cells.

Our results indicate that p53 hyperactivation induced by CHD8 loss elicits not only cell cycle arrest and apoptosis but also a differentiation block in HSCs. Our RNA sequencing data showed that CHD8 loss did not affect the expression of HSC-related gene sets, suggesting that stem cell identity was not substantially affected by CHD8 deficiency, even though stemness was substantially impaired in *Chd8*$^{\Delta/\Delta}$ HSCs as revealed by the inability of these cells to reconstruct the hematopoietic system after BM transplantation *in vivo* as well as by their defective self-renewal and differentiation abilities in colony-formation assays *in vitro*. The transition from HSCs to multipotent progenitor cells is thus likely blocked by unrestrained p53 activity as a result of CHD8 loss. Additional ablation of p53 released the differentiation block between CD48$^-$CD150$^+$ LSK cells and CD48$^-$CD150$^-$ LSK and Flt3$^+$CD34$^+$ LSK cells in *Chd8*$^{\Delta/\Delta}$ mice, suggesting that p53 antagonizes these differentiation steps. A similar release of a differentiation block by *Trp53* deletion has been observed in a previous study. The number of HSCs in Wip1-deficient mice was thus found to be increased as a result of a differentiation block that was released by additional p53 ablation (Chen et al., 2015). We thus conclude that CHD8 antagonizes p53 activity at the steady state and thereby contributes to maintenance of the balance between self-renewal and differentiation of HSCs.

CHD8 is implicated as a causative gene for ASD, and the role of CHD8 in neurodevelopment has been well characterized. However, few evaluations of its function in stem cells of other tissues have been undertaken. We have now found that CHD8 is indispensable for HSC function, suggesting that more extensive analysis of its role in other stem cell systems is warranted. In particular, given that p53 plays a central role in regulation of carcinogenesis and cell senescence, the contribution of CHD8 to such processes needs to be investigated.

STAR★METHODS

Detailed methods are provided in the online version of this paper and include the following:

- KEY RESOURCES TABLE
- RESOURCE AVAILABILITY
  - Lead contact
  - Materials availability
  - Data and code availability
- EXPERIMENTAL MODEL AND SUBJECT DETAILS
  - Animals
- METHOD DETAILS
  - Flow cytometric analysis and cell sorting
  - Detection of apoptosis
  - BM reconstitution assay
  - Colony formation assay
  - RT and real-time PCR analysis
  - ChIP-qPCR
  - RNA-sequencing analysis
  - Immunoblot analysis
  - Immunofluorescence staining
  - Hematologic and biochemical analyses
- QUANTIFICATION AND STATISTICAL ANALYSIS

SUPPLEMENTAL INFORMATION

Supplemental Information can be found online at https://doi.org/10.1016/j.celrep.2021.108688.

ACKNOWLEDGMENTS

We thank T. Akinaga, K. Tsunematsu, L. Cui, and other laboratory members for technical assistance, as well as A. Ohta for help with preparation of the manuscript. This study was supported in part by KAKENHI grants (18H05215 and 19H05220) from the Ministry of Education, Culture, Sports, Science, and Technology of Japan, Japan.

AUTHOR CONTRIBUTIONS

Conceptualization, A.N., M.N., and K.I.N.; Methodology, A.N.; Formal Analysis, A.N.; Investigation, A.N. and Y.M.; Resources, Y.K.; Writing – Original Draft, A.N., A.M., and K.I.N.; Writing – Review & Editing, A.N., Y.K., and K.I.N.; Visualization, A.N.; Project Administration, K.I.N.; Funding Acquisition, K.I.N.

DECLARATION OF INTERESTS

The authors declare no competing interests.

Received: March 10, 2020
Revised: October 26, 2020
Accepted: December 30, 2020
Published: February 2, 2021

Figure 5. Additional p53 ablation releases the differentiation block of *Chd8*$^{\Delta/\Delta}$ HSCs

(A) Number of BM cells in control (n = 5), *Trp53*$^{-/-}$ (n = 4), *Chd8*$^{\Delta/\Delta}$ (n = 7), and *Trp53*$^{-/-}$/*Chd8*$^{\Delta/\Delta}$ (n = 5) mice at 4 weeks after the last poly(I:C) injection. Data are presented as box-and-whisker plots. N.S. (Student's t test).

(B–E) Representative flow cytometric analysis of Lin$^-$ cells (B), Lin$^-$CD127$^-$c-Kit$^+$ cells (C), Lin$^-$CD127$^+$ cells (D), and LSK cells (E) isolated from BM mononuclear cells of control, *Trp53*$^{-/-}$, *Chd8*$^{\Delta/\Delta}$, and *Trp53*$^{-/-}$/*Chd8*$^{\Delta/\Delta}$ mice at 4 weeks after the last poly(I:C) injection.

(F–H) Total cell number for LSK, LK, and LS cells (F); CLP, GMP, CMP, and MEP cells (G); as well as CD48$^-$CD150$^+$ LSK, CD48$^+$CD150$^+$ LSK, CD48$^+$CD150$^-$ LSK, CD48$^-$CD150$^-$ LSK, Flt3$^-$CD34$^-$ LSK, Flt3$^-$CD34$^+$ LSK, and Flt3$^+$CD34$^+$ LSK (H) cells among BM cells of control (n = 5), *Trp53*$^{-/-}$ (n = 4), *Chd8*$^{\Delta/\Delta}$ (n = 7), and *Trp53*$^{-/-}$/*Chd8*$^{\Delta/\Delta}$ (n = 5) mice at 4 weeks after the last poly(I:C) injection. Data are presented as box-and-whicker plots. *p < 0.05; **p < 0.01; ***p < 0.005; N.S. (Student's t test).

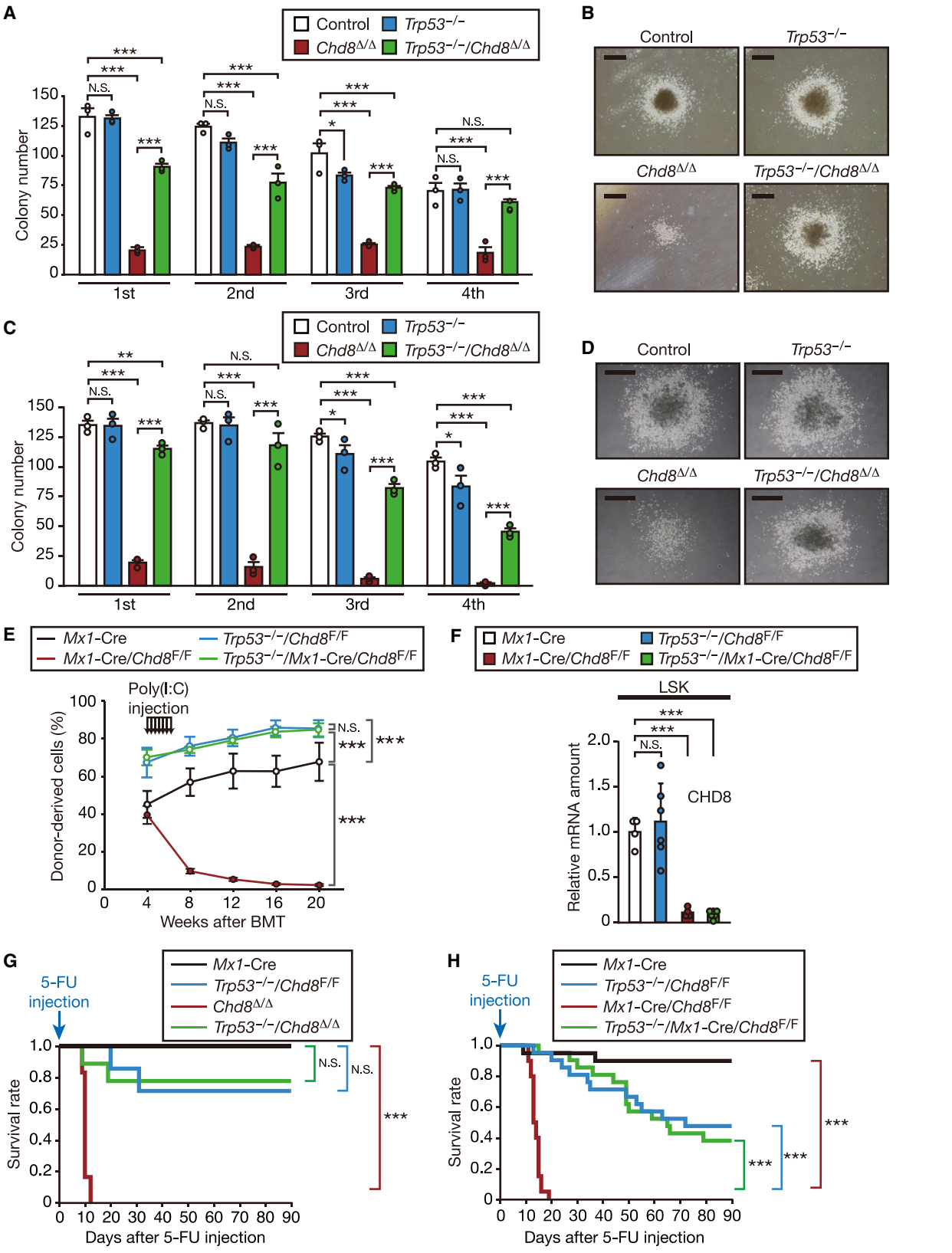

(legend on next page)

REFERENCES

Akala, O.O., Park, I.K., Qian, D., Pihalja, M., Becker, M.W., and Clarke, M.F. (2008). Long-term haematopoietic reconstitution by Trp53-/-p16Ink4a-/-p19Arf-/- multipotent progenitors. Nature *453*, 228–232.

Allen, M.A., Andrysik, Z., Dengler, V.L., Mellert, H.S., Guarnieri, A., Freeman, J.A., Sullivan, K.D., Galbraith, M.D., Luo, X., Kraus, W.L., et al. (2014). Global analysis of p53-regulated transcription identifies its direct targets and unexpected regulatory mechanisms. eLife *3*, e02200.

Artinger, E.L., Mishra, B.P., Zaffuto, K.M., Li, B.E., Chung, E.K., Moore, A.W., Chen, Y., Cheng, C., and Ernst, P. (2013). An MLL-dependent network sustains hematopoiesis. Proc. Natl. Acad. Sci. USA *110*, 12000–12005.

Avgustinova, A., and Benitah, S.A. (2016). Epigenetic control of adult stem cell function. Nat. Rev. Mol. Cell Biol. *17*, 643–658.

Bernier, R., Golzio, C., Xiong, B., Stessman, H.A., Coe, B.P., Penn, O., Witherspoon, K., Gerdts, J., Baker, C., Vulto-van Silfhout, A.T., et al. (2014). Disruptive CHD8 mutations define a subtype of autism early in development. Cell *158*, 263–276.

Bolger, A.M., Lohse, M., and Usadel, B. (2014). Trimmomatic: a flexible trimmer for Illumina sequence data. Bioinformatics *30*, 2114–2120.

Bröske, A.M., Vockentanz, L., Kharazi, S., Huska, M.R., Mancini, E., Scheller, M., Kuhl, C., Enns, A., Prinz, M., Jaenisch, R., et al. (2009). DNA methylation protects hematopoietic stem cell multipotency from myeloerythroid restriction. Nat. Genet. *41*, 1207–1215.

Butler, J.S., and Dent, S.Y.R. (2013). The role of chromatin modifiers in normal and malignant hematopoiesis. Blood *121*, 3076–3084.

Cedar, H., and Bergman, Y. (2011). Epigenetics of haematopoietic cell development. Nat. Rev. Immunol. *11*, 478–488.

Chapple, R.H., Hu, T., Tseng, Y.J., Liu, L., Kitano, A., Luu, V., Hoegenauer, K.A., Iwawaki, T., Li, Q., and Nakada, D. (2018). ERα promotes murine hematopoietic regeneration through the Ire1α-mediated unfolded protein response. eLife *7*, 31159.

Chen, J., Ellison, F.M., Keyvanfar, K., Omokaro, S.O., Desierto, M.J., Eckhaus, M.A., and Young, N.S. (2008). Enrichment of hematopoietic stem cells with SLAM and LSK markers for the detection of hematopoietic stem cell function in normal and Trp53 null mice. Exp. Hematol. *36*, 1236–1243.

Chen, Z., Yi, W., Morita, Y., Wang, H., Cong, Y., Liu, J.P., Xiao, Z., Rudolph, K.L., Cheng, T., and Ju, Z. (2015). Wip1 deficiency impairs haematopoietic stem cell function via p53 and mTORC1 pathways. Nat. Commun. *6*, 6808.

Clapier, C.R., and Cairns, B.R. (2009). The biology of chromatin remodeling complexes. Annu. Rev. Biochem. *78*, 273–304.

Cui, K., Zang, C., Roh, T.Y., Schones, D.E., Childs, R.W., Peng, W., and Zhao, K. (2009). Chromatin signatures in multipotent human hematopoietic stem cells indicate the fate of bivalent genes during differentiation. Cell Stem Cell *4*, 80–93.

de Dieuleveult, M., Yen, K., Hmitou, I., Depaux, A., Boussouar, F., Bou Dargham, D., Jounier, S., Humbertclaude, H., Ribierre, F., Baulard, C., et al. (2016). Genome-wide nucleosome specificity and function of chromatin remodellers in ES cells. Nature *530*, 113–116.

Dietrich, P.A., Yang, C., Leung, H.H., Lynch, J.R., Gonzales, E., Liu, B., Haber, M., Norris, M.D., Wang, J., and Wang, J.Y. (2014). GPR84 sustains aberrant β-catenin signaling in leukemic stem cells for maintenance of MLL leukemogenesis. Blood *124*, 3284–3294.

Fischer, M. (2017). Census and evaluation of p53 target genes. Oncogene *36*, 3943–3956.

Fischer, M. (2019). Conservation and divergence of the p53 gene regulatory network between mice and humans. Oncogene *38*, 4095–4109.

Flach, J., Bakker, S.T., Mohrin, M., Conroy, P.C., Pietras, E.M., Reynaud, D., Alvarez, S., Diolaiti, M.E., Ugarte, F., Forsberg, E.C., et al. (2014). Replication stress is a potent driver of functional decline in ageing haematopoietic stem cells. Nature *512*, 198–202.

Hatakeyama, S., Matsumoto, M., Kamura, T., Murayama, M., Chui, D.H., Planel, E., Takahashi, R., Nakayama, K.I., and Takashima, A. (2004). U-box protein carboxyl terminus of Hsc70-interacting protein (CHIP) mediates polyubiquitylation preferentially on four-repeat Tau and is involved in neurodegeneration of tauopathy. J. Neurochem. *91*, 299–307.

Katayama, Y., Nishiyama, M., Shoji, H., Ohkawa, Y., Kawamura, A., Sato, T., Suyama, M., Takumi, T., Miyakawa, T., and Nakayama, K.I. (2016). CHD8 haploinsufficiency results in autistic-like phenotypes in mice. Nature *537*, 675–679.

Kita, Y., Katayama, Y., Shiraishi, T., Oka, T., Sato, T., Suyama, M., Ohkawa, Y., Miyata, K., Oike, Y., Shirane, M., et al. (2018). The autism-related protein CHD8 cooperates with C/EBPβ to regulate adipogenesis. Cell Rep. *23*, 1988–2000.

Kühn, R., Schwenk, F., Aguet, M., and Rajewsky, K. (1995). Inducible gene targeting in mice. Science *269*, 1427–1429.

Lawrence, M., Gentleman, R., and Carey, V. (2009). rtracklayer: an R package for interfacing with genome browsers. Bioinformatics *25*, 1841–1842.

Liao, Y., Smyth, G.K., and Shi, W. (2019). The R package Rsubread is easier, faster, cheaper and better for alignment and quantification of RNA sequencing reads. Nucleic Acids Res. *47*, e47.

Liu, Y., Elf, S.E., Asai, T., Miyata, Y., Liu, Y., Sashida, G., Huang, G., Di Giandomenico, S., Koff, A., and Nimer, S.D. (2009a). The p53 tumor suppressor protein is a critical regulator of hematopoietic stem cell behavior. Cell Cycle *8*, 3120–3124.

Liu, Y., Elf, S.E., Miyata, Y., Sashida, G., Liu, Y., Huang, G., Di Giandomenico, S., Lee, J.M., Deblasio, A., Menendez, S., et al. (2009b). p53 regulates hematopoietic stem cell quiescence. Cell Stem Cell *4*, 37–48.

Love, M.I., Huber, W., and Anders, S. (2014). Moderated estimation of fold change and dispersion for RNA-seq data with DESeq2. Genome Biol. *15*, 550.

Matatall, K.A., Kadmon, C.S., and King, K.Y. (2018). Detecting hematopoietic stem cell proliferation using BrdU incorporation. Methods Mol. Biol. *1686*, 91–103.

Matsumoto, A., Takeishi, S., Kanie, T., Susaki, E., Onoyama, I., Tateishi, Y., Nakayama, K., and Nakayama, K.I. (2011). p57 is required for quiescence and maintenance of adult hematopoietic stem cells. Cell Stem Cell *9*, 262–271.

Figure 6. Stem cell capacity is restored by p53 ablation in *Chd8*$^{\Delta/\Delta}$ HSCs both *in vitro* and *in vivo*

(A–D) Colony-formation assay for control, *Trp53*$^{-/-}$, *Chd8*$^{\Delta/\Delta}$, and *Trp53*$^{-/-}$/*Chd8*$^{\Delta/\Delta}$ LSK cells (A) and long-term HSCs (C). Data are means ± SD (n = 3 independent experiments). *p < 0.05; **p < 0.01; ***p < 0.005; N.S. (Student's t test). Representative colonies for (A) and (C) are shown in (B) and (D), respectively. Scale bars, 0.5 mm.

(E) Donor BM cells (4 × 10^5) from control (n = 4), *Trp53*$^{-/-}$/*Chd8*$^{F/F}$ (n = 6), *Mx1-Cre*/*Chd8*$^{F/F}$ (n = 4), or *Trp53*$^{-/-}$/*Mx1-Cre*/*Chd8*$^{F/F}$ (n = 6) mice were transplanted together with an equal number of competitor BM cells into lethally irradiated recipient mice, which were injected with poly(I:C) beginning 4 weeks after BM transfer. The percentage of donor-derived cells in PB at the indicated times after BM transfer was determined. Data are means ± SD. ***p < 0.005; N.S. (Student's t test).

(F) RT and real-time PCR analysis of CHD8 mRNA in LSK cells at 20 weeks after BM transfer as in (E). Data are means ± SD. ***p < 0.005; N.S. (Student's t test).

(G) Survival rate of control (n = 7), *Trp53*$^{-/-}$/*Chd8*$^{F/F}$ (n = 7), *Chd8*$^{\Delta/\Delta}$ (n = 6), and *Trp53*$^{-/-}$/*Chd8*$^{\Delta/\Delta}$ (n = 9) mice after 5-FU (150 mg/kg) injection at 4 weeks after the last poly(I:C) injection. ***p < 0.005; N.S. (log rank test).

(H) Donor BM cells (1 × 10^6) from control (n = 20), *Trp53*$^{-/-}$/*Chd8*$^{F/F}$ (n = 21), *Mx1-Cre*/*Chd8*$^{F/F}$ (n = 20), or *Trp53*$^{-/-}$/*Mx1-Cre*/*Chd8*$^{F/F}$ (n = 21) mice were transplanted into lethally irradiated recipient mice, which were injected with poly(I:C) beginning 4 weeks after BM transfer. The survival rate of the recipients was determined after their injection with 5-FU (150 mg/kg) at 4 weeks after the last poly(I:C) injection. ***p < 0.005 (log rank test).

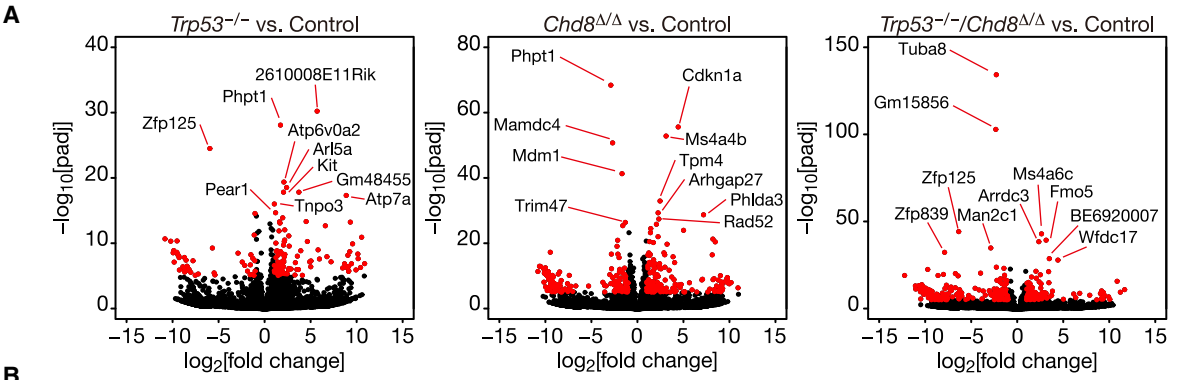

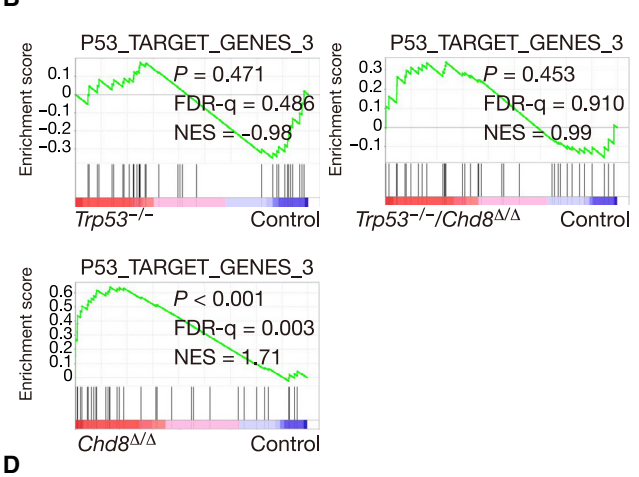

C

Gene set	NES	NOM *P* value	FDR *q* value
P53_TARGET_GENES_1			
Trp53$^{-/-}$ vs. Control	-1.07	0.300	0.431
Chd8$^{\Delta/\Delta}$ vs. Control	1.62	< 0.001	0.003
Trp53$^{-/-}$/*Chd8*$^{\Delta/\Delta}$ vs. Control	-1.61	0.005	0.023
P53_TARGET_GENES_2			
Trp53$^{-/-}$ vs. Control	-1.13	0.194	0.458
Chd8$^{\Delta/\Delta}$ vs. Control	1.68	< 0.001	0.002
Trp53$^{-/-}$/*Chd8*$^{\Delta/\Delta}$ vs. Control	-1.20	0.147	0.382
P53_TARGET_GENES_3			
Trp53$^{-/-}$ vs. Control	-0.98	0.471	0.486
Chd8$^{\Delta/\Delta}$ vs. Control	1.71	< 0.001	0.003
Trp53$^{-/-}$/*Chd8*$^{\Delta/\Delta}$ vs. Control	0.99	0.453	0.910

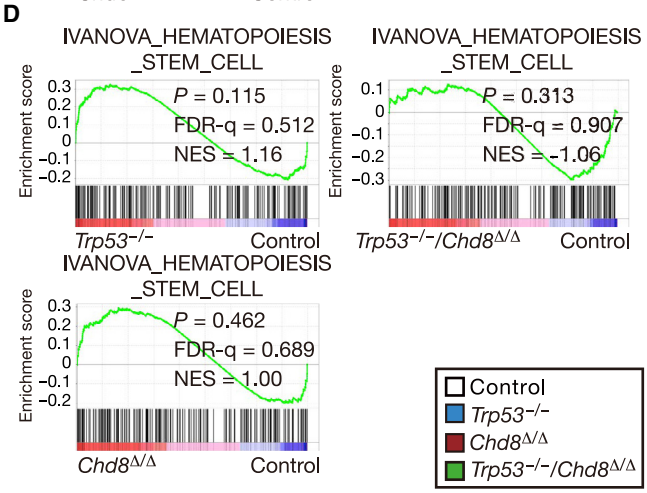

E

Gene set	NES	NOM *P* value	FDR *q* value
IVANOVA_HEMATOPOIESIS_STEM_CELL			
Trp53$^{-/-}$ vs. Control	1.16	0.115	0.512
Chd8$^{\Delta/\Delta}$ vs. Control	1.00	0.462	0.689
Trp53$^{-/-}$/*Chd8*$^{\Delta/\Delta}$ vs. Control	-1.06	0.313	0.907
CONRAD_STEM_CELL			
Trp53$^{-/-}$ vs. Control	0.87	0.672	0.962
Chd8$^{\Delta/\Delta}$ vs. Control	0.99	0.469	0.754
Trp53$^{-/-}$/*Chd8*$^{\Delta/\Delta}$ vs. Control	0.77	0.887	0.989
BYSTRYKH_HEMATOPOIESIS_STEM_CELL_QTL_CIS			
Trp53$^{-/-}$ vs. Control	0.81	0.948	0.994
Chd8$^{\Delta/\Delta}$ vs. Control	0.89	0.728	0.873
Trp53$^{-/-}$/*Chd8*$^{\Delta/\Delta}$ vs. Control	1.12	0.176	0.624

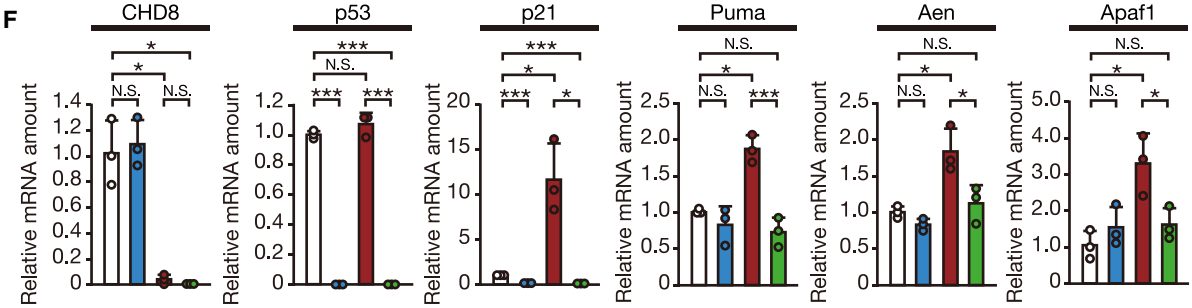

(legend on next page)

Micucci, J.A., Sperry, E.D., and Martin, D.M. (2015). Chromodomain helicase DNA-binding proteins in stem cells and human developmental diseases. Stem Cells Dev. *24*, 917–926.

Miyamoto, K., Araki, K.Y., Naka, K., Arai, F., Takubo, K., Yamazaki, S., Matsuoka, S., Miyamoto, T., Ito, K., Ohmura, M., et al. (2007). Foxo3a is essential for maintenance of the hematopoietic stem cell pool. Cell Stem Cell *1*, 101–112.

Muto, Y., Nishiyama, M., Nita, A., Moroishi, T., and Nakayama, K.I. (2017). Essential role of FBXL5-mediated cellular iron homeostasis in maintenance of hematopoietic stem cells. Nat. Commun. *8*, 16114.

Nagarajan, P., Onami, T.M., Rajagopalan, S., Kania, S., Donnell, R., and Venkatachalam, S. (2009). Role of chromodomain helicase DNA-binding protein 2 in DNA damage response signaling and tumorigenesis. Oncogene *28*, 1053–1062.

Neale, B.M., Kou, Y., Liu, L., Ma'ayan, A., Samocha, K.E., Sabo, A., Lin, C.F., Stevens, C., Wang, L.S., Makarov, V., et al. (2012). Patterns and rates of exonic de novo mutations in autism spectrum disorders. Nature *485*, 242–245.

Nishiyama, M., Oshikawa, K., Tsukada, Y., Nakagawa, T., Iemura, S., Natsume, T., Fan, Y., Kikuchi, A., Skoultchi, A.I., and Nakayama, K.I. (2009). CHD8 suppresses p53-mediated apoptosis through histone H1 recruitment during early embryogenesis. Nat. Cell Biol. *11*, 172–182.

Nishiyama, M., Skoultchi, A.I., and Nakayama, K.I. (2012). Histone H1 recruitment by CHD8 is essential for suppression of the Wnt-β-catenin signaling pathway. Mol. Cell. Biol. *32*, 501–512.

Nita, A., Nishiyama, M., Muto, Y., and Nakayama, K.I. (2016). FBXL12 regulates T-cell differentiation in a cell-autonomous manner. Genes Cells *21*, 517–524.

O'Roak, B.J., Vives, L., Girirajan, S., Karakoc, E., Krumm, N., Coe, B.P., Levy, R., Ko, A., Lee, C., Smith, J.D., et al. (2012a). Sporadic autism exomes reveal a highly interconnected protein network of de novo mutations. Nature *485*, 246–250.

O'Roak, B.J., Vives, L., Fu, W., Egertson, J.D., Stanaway, I.B., Phelps, I.G., Carvill, G., Kumar, A., Lee, C., Ankenman, K., et al. (2012b). Multiplex targeted sequencing identifies recurrently mutated genes in autism spectrum disorders. Science *338*, 1619–1622.

Pant, V., Quintás-Cardama, A., and Lozano, G. (2012). The p53 pathway in hematopoiesis: lessons from mouse models, implications for humans. Blood *120*, 5118–5127.

Prasad, P., Lennartsson, A., and Ekwall, K. (2015). The roles of SNF2/SWI2 nucleosome remodeling enzymes in blood cell differentiation and leukemia. BioMed Res. Int. *2015*, 347571.

Sakamoto, I., Kishida, S., Fukui, A., Kishida, M., Yamamoto, H., Hino, S., Michiue, T., Takada, S., Asashima, M., and Kikuchi, A. (2000). A novel β-catenin-binding protein inhibits β-catenin-dependent Tcf activation and axis formation. J. Biol. Chem. *275*, 32871–32878.

Seita, J., and Weissman, I.L. (2010). Hematopoietic stem cell: self-renewal versus differentiation. Wiley Interdiscip. Rev. Syst. Biol. Med. *2*, 640–653.

Solozobova, V., and Blattner, C. (2011). p53 in stem cells. World J. Biol. Chem. *2*, 202–214.

Subramanian, A., Tamayo, P., Mootha, V.K., Mukherjee, S., Ebert, B.L., Gillette, M.A., Paulovich, A., Pomeroy, S.L., Golub, T.R., Lander, E.S., and Mesirov, J.P. (2005). Gene set enrichment analysis: a knowledge-based approach for interpreting genome-wide expression profiles. Proc. Natl. Acad. Sci. USA *102*, 15545–15550.

Takahashi, H., Hatakeyama, S., Saitoh, H., and Nakayama, K.I. (2005). Noncovalent SUMO-1 binding activity of thymine DNA glycosylase (TDG) is required for its SUMO-1 modification and colocalization with the promyelocytic leukemia protein. J. Biol. Chem. *280*, 5611–5621.

Talkowski, M.E., Rosenfeld, J.A., Blumenthal, I., Pillalamarri, V., Chiang, C., Heilbut, A., Ernst, C., Hanscom, C., Rossin, E., Lindgren, A.M., et al. (2012). Sequencing chromosomal abnormalities reveals neurodevelopmental loci that confer risk across diagnostic boundaries. Cell *149*, 525–537.

TeKippe, M., Harrison, D.E., and Chen, J. (2003). Expansion of hematopoietic stem cell phenotype and activity in Trp53-null mice. Exp. Hematol. *31*, 521–527.

Wilson, A., Laurenti, E., Oser, G., van der Wath, R.C., Blanco-Bose, W., Jaworski, M., Offner, S., Dunant, C.F., Eshkind, L., Bockamp, E., et al. (2008). Hematopoietic stem cells reversibly switch from dormancy to self-renewal during homeostasis and repair. Cell *135*, 1118–1129.

Wilson, N.K., Schoenfelder, S., Hannah, R., Sánchez Castillo, M., Schütte, J., Ladopoulos, V., Mitchelmore, J., Goode, D.K., Calero-Nieto, F.J., Moignard, V., et al. (2016). Integrated genome-scale analysis of the transcriptional regulatory landscape in a blood stem/progenitor cell model. Blood *127*, e12–e23.

Yamashita, M., Nitta, E., and Suda, T. (2016). Regulation of hematopoietic stem cell integrity through p53 and its related factors. Ann. N Y Acad. Sci. *1370*, 45–54.

Yoshida, T., Hazan, I., Zhang, J., Ng, S.Y., Naito, T., Snippert, H.J., Heller, E.J., Qi, X., Lawton, L.N., and Williams, C.J. (2008). The role of the chromatin remodeler Mi-2β in hematopoietic stem cell self-renewal and multilineage differentiation. Genes Dev. *22*, 1174–1189.

Figure 7. CHD8-deficiency-induced, p53-dependent differentiation block from HSCs to progenitors

(A) Volcano plots of differentially expressed genes in *Trp53*$^{-/-}$, *Chd8*$^{\Delta/\Delta}$, or *Trp53*$^{-/-}$/*Chd8*$^{\Delta/\Delta}$ HSCs compared with control HSCs at 4 weeks after the last poly(I:C) injection. Differentially expressed genes with an adjusted $p < 0.00001$ and $\log_2$[fold change] of >1 or <−1 are shown as red dots, and the names of the 10 genes with the largest $-\log_{10}$[padj] value among these genes are indicated.

(B–E) GSEA plots for p53-pathway-related (B) or HSC- or stem-cell-related (D) gene sets, as well as summaries of such analysis (C and E), in *Trp53*$^{-/-}$, *Chd8*$^{\Delta/\Delta}$, or *Trp53*$^{-/-}$/*Chd8*$^{\Delta/\Delta}$ HSCs compared with control HSCs at 4 weeks after the last poly(I:C) injection.

(F) RT and real-time PCR analysis of CHD8, p53, and p53 target gene mRNAs in control, *Trp53*$^{-/-}$, *Chd8*$^{\Delta/\Delta}$, and *Trp53*$^{-/-}$/*Chd8*$^{\Delta/\Delta}$ HSCs at 4 weeks after the last poly(I:C) injection. Normalized data are expressed relative to the value for control cells. Data are means ± SD (n = 3 mice). *$p < 0.05$; ***$p < 0.005$; N.S. (Student's t test).

See also Tables S2–S4.

STAR★METHODS

KEY RESOURCES TABLE

REAGENT or RESOURCE	SOURCE	IDENTIFIER
Antibodies		
Rabbit polyclonal anti–CHD8	(Nishiyama et al., 2009)	N/A
Rat monoclonal anti–CHD8	(Katayama et al., 2016)	N/A
Phospho–Histone H2A.X (Ser139)	Cell Signaling Technology	Cat#2577; RRID: AB_2118010
AffiniPure Rabbit anti–Rat IgG (H+L)	Jackson ImmunoResearch	Cat#312–005–003; RRID: AB_2339800
Normal Rat IgG	Santa Cruz Biotechnology	Cat#sc–2026; RRID: AB_737202
APC Mouse Anti–CD45.1 (A20)	BD Biosciences	Cat#558701; RRID: AB_1645214
Biotin Mouse Anti–CD45.2 (104)	BD Biosciences	Cat#553771; RRID: AB_395040
Biotin Mouse Anti–CD127 (Il–7ra)	BioLegend	Cat#351346; RRID: AB_2566509
PE–Cy7 Rat Anti–Mouse Ly–6A/E (D7)	BD Biosciences	Cat#558162; RRID: AB_647253
APC Rat Anti–Mouse CD117 (2B8)	BD Biosciences	Cat#553356; RRID: AB_398536
Biotin Anti–Mouse CD48 (HM48–1)	BioLegend	Cat#103410; RRID: AB_528827
PE Anti–Mouse CD150 (SLAM) (TC15–12F12.2)	BioLegend	Cat#115904; RRID: AB_313683
PE–Cy5 Hamster Anti–Mouse CD3e (145–2C11)	BD Biosciences	Cat#553065; RRID: AB_394598
PE–Cy5 Rat Anti–Mouse CD4 (RM4–5)	BD Biosciences	Cat#561836; RRID: AB_10894584
PE–Cy5 Rat Anti–Mouse CD8a (53–6.7)	BD Biosciences	Cat#553034; RRID: AB_394572
PE–Cy5 Rat Anti–Mouse CD45R/B220 (RA3–6B2)	BD Biosciences	Cat#553091; RRID: AB_394621
PE–Cy5 Rat Anti–Mouse Ly–6G/Ly–6C (Gr–1) (RB6–8C5)	BioLegend	Cat#108410; RRID: AB_313375
PE–Cy5 Rat Anti–Mouse/Human CD11b (M1/70)	BioLegend	Cat#101210; RRID: AB_312793
PE–Cy5 Rat Anti–Mouse TER119/Erythroid Cells (TER–119)	BioLegend	Cat#116210; RRID: AB_313711
FITC Hamster Anti–Mouse CD3e (145–2C11)	BD Biosciences	Cat#553062; RRID: AB_394595
PE Rat Anti–Mouse CD45R/B220 (RA3–6B2)	BD Biosciences	Cat#553090; RRID: AB_394620
FITC Rat Anti-Mouse Ly–6G and Ly–6C (RB6–8C5)	BD Biosciences	Cat#553127; RRID: AB_394643
PE Rat Anti–Mouse CD11b (M1/70)	BD Biosciences	Cat#557397; RRID: AB_396680
FITC Rat Anti–Mouse CD16/CD32 (93)	BioLegend	Cat#101305; RRID: AB_312804
PE Rat Anti–Mouse CD135 (A2F10.1)	BD Biosciences	Cat#553842; RRID: AB_395079
Pacific Blue Rat anti–Mouse CD34 (RAM34)	eBioscience	Cat#48–0341–82; RRID: AB_2043837
Alexa Fluor 488 Anti-Mouse Ki–67 (16A8)	BioLegend	Cat#652417; RRID: AB_2564236
FITC Annexin V	BioLegend	Cat#640906
Streptavidin PE–Cy7	BD Biosciences	Cat#557598; RRID: AB_10049577
Streptavidin APC–Cy7	BD Biosciences	Cat#554063; RRID: AB_10054651
Anti–Smooth Muscle Actin (CGA7)	Santa Cruz Biotechnology	Cat#sc–53015; RRID: AB_628683
Anti–Mouse IgG, HRP–conjugated	Promega	Cat#W4021; RRID: AB_430834
Anti–Rabbit IgG, HRP–conjugated	Promega	Cat#W4011: RRID: AB_430833
Alexa Fluor 488–conjugated goat Anti–Rabbit IgG	Thermo Fischer Scientific	Cat#A–11034; RRID: AB_2576217

(*Continued on next page*)

Continued

REAGENT or RESOURCE	SOURCE	IDENTIFIER
Chemicals, peptides, and recombinant proteins		
Hoechst33342	Thermo Fisher Scientific	Cat#H21492
DAPI	Sigma	Cat#D9542
LIVE/DEAD Fixable Near-IR Dead Cell Stain Kit, for 633 or 635 nm excitation	Thermo Fisher Scientific	Cat#L10119
Poly (I:C)	Tocris Bioscience	Cat#4287
5–Fluorouracil	Merck	Cat#F6627
BrdU	Merck	Cat#B5002
Propidium Iodide	Merck	Cat#P4170
Isogen	Nippon Gene	Cat#317–02503
Ethachinmate	Nippon Gene	Cat#312–01791
Poly–L–lysine	Sigma	Cat#8920
Fluoromount	Diagnoistic BioSystems	Cat#K024
cOmplete, EDTA–free Protease Inhibitor Cocktail Tablets	Roche	Cat#11873580001
Critical commercial assays		
QuantiTect Reverse Transcription Kit	QIAGEN	Cat#205311
SYBR Green PCR Master Mix	Thermo Fisher Scientific	Cat#4309155
MethoCult GF M3434	STEMCELL Technologies	Cat#03434
Dynabeads M–280 Sheep anti–Rabbit IgG	Invitrogen	Cat#DB11204
MinElute PCR purification kit	QIAGEN	Cat#28006
Nucleo Spin RNA XS	Takara Bio	Cat#740902–50
SMART–seq v4 Ultra Low Input RNA Kit	Takara Bio	Cat#634890
Nextera XT DNA Sample Preparation Kit	Illumina	Cat#FC–131–1024
Nextera XT Index Kit	Illumina	Cat#FC–131–1001
FITC Mouse Anti–BrdU Set	BD Biosciences	Cat#556028; RRID: AB_396304
10 × Annexin V Binding Buffer	BD Biosciences	Cat#51–66121E
Deposited data		
RNA-sequencing raw data	This study	DRA010864
Experimental models: cell lines		
Mouse: OP9 cells	RIKEN cell bank	N/A
Experimental models: organisms/strains		
Mouse: C57BL/6JJcl	Japan Clea	N/A
Mouse: *Chd8* Flox	(Katayama et al., 2016)	N/A
Mouse: B6; *Trp53* KO	(Nishiyama et al., 2009)	N/A
Mouse: B6; *Mx1-Cre*/J	(Kühn et al., 1995)	N/A
Mouse: B6; CD45.1 congenic	The Jackson Laboratory	Cat#002014
Oligonucleotides		
See Table S5 for oligonucleotide information	This study	N/A
Software and algorithms		
FastQC (version 0.11.9)	Babraham institute	https://www.bioinformatics.babraham.ac.uk/projects/fastqc
Trimmomatic (Version 0.39)	(Bolger et al., 2014)	http://www.usadellab.org/cms/?page=trimmomatic
HISAT2.1.0	Laboratory of Daehwan Kim	http://daehwankimlab.github.io/hisat2/
Rsubread	(Liao et al., 2019)	https://bioconductor.org/packages/release/bioc/html/Rsubread.html

(*Continued on next page*)

Continued

REAGENT or RESOURCE	SOURCE	IDENTIFIER
DESeq2 (version 3.11)	(Love et al., 2014)	http://cole-trapnell-lab.github.io/cufflinks/
rtracklayer	(Lawrence et al., 2009)	https://bioconductor.org/packages/release/bioc/html/rtracklayer.html
GSEA (version 4.1.0)	(Subramanian et al., 2005)	https://www.gsea-msigdb.org/gsea/index.jsp
JMP Pro software	SAS	https://www.jmp.com/ja_jp/home.html

RESOURCE AVAILABILITY

Lead contact

Further information and requests for resources and reagents should be directed to and will be fulfilled by the Lead Contact, Keiichi I. Nakayama (nakayak1@bioreg.kyushu-u.ac.jp).

Materials availability

Mice homozygous for a floxed allele of *Chd8* (*Chd8*$^{F/F}$ mice) used in this study are available from the Experimental Animal Division, RIKEN BioResource Research Center (https://mus.brc.riken.jp/en/). Commercially available reagents are indicated in the Key resources table.

Data and code availability

The accession number for the RNA-sequencing data reported in this paper is DRA: DRA010864.DRA010864

EXPERIMENTAL MODEL AND SUBJECT DETAILS

Animals

Generation of mice homozygous for a floxed allele of *Chd8* (*Chd8*$^{F/F}$ mice) was described previously (Katayama et al., 2016). These mice were crossed with *Mx1-Cre* transgenic mice (Kühn et al., 1995) or *Trp53*$^{-/-}$ mice to generate *Mx1-Cre*/*Chd8*$^{F/F}$ and *Trp53*$^{-/-}$/*Mx1-Cre*/*Chd8*$^{F/F}$ mice. All of these mice were backcrossed with C57BL/6 mice for > 10 generations. Expression of Cre recombinase in mice harboring the *Mx1-Cre* transgene was induced by intraperitoneal injection of poly(I:C) at a dose of 20 mg/kg on seven alternate days beginning at 8 weeks of age. *Mx1-Cre*/*Chd8*$^{F/F}$ mice and *Trp53*$^{-/-}$/*Mx1-Cre*/*Chd8*$^{F/F}$ mice were analyzed 4 weeks after the last poly(I:C) injection, unless indicated otherwise. For some experiments, mice were injected intraperitoneally with 5-FU at a dose of 150 mg/kg. All mouse experiments were approved by the Animal Ethics Committee of Kyushu University.

METHOD DETAILS

Flow cytometric analysis and cell sorting

Flow cytometric analysis and fluorescence-activated cell sorting (FACS) were performed with the use of FACSVerse or FACSAria instruments (BD Biosciences). CD3ε, CD4, CD8, B220, Ter119, Gr1, and Mac1 were adopted as lineage markers. For analysis of HSCs, antibodies to lineage markers were used at a 1:60 dilution and other antibodies at a 1:50 dilution. For analysis of differentiated cells, all antibodies were used at a 1:100 dilution. BM mononuclear cells flushed from the tibia and femur of mice were suspended in phosphate-buffered saline (PBS) supplemented with 2% heat-inactivated fetal bovine serum (FBS), incubated with the indicated antibodies for 30 min on ice, washed, and then analyzed. For intracellular staining of Ki-67, cells were stained for surface markers, fixed in PBS containing 2% paraformaldehyde for 20 min, permeabilized with PBS containing 0.5% saponin and 0.5% bovine serum albumin for 10 min at room temperature, and then incubated with the antibodies to Ki-67. For analysis of the cell cycle, cells stained with antibodies to Ki-67 were briefly exposed to Hoechst 33342 before analysis. Analysis of BrdU incorporation in LSK cells was performed as previously described (Matatall et al., 2018).

Detection of apoptosis

For assay of apoptosis, BM cells stained with antibodies to cell surface markers were further stained for 15 min at room temperature with annexin V and propidium iodide with the use of 10 × Annexin V Binding Buffer.

BM reconstitution assay

A BM reconstitution assay was performed as previously described (Nita et al., 2016). Unless indicated otherwise, unfractionated BM cells (4×10^5) isolated from control, *Trp53*$^{-/-}$/*Chd8*$^{F/F}$, *Mx1-Cre*/*Chd8*$^{F/F}$, or *Trp53*$^{-/-}$/*Mx1-Cre*/*Chd8*$^{F/F}$ mice (CD45.2) at 4 weeks after poly(I:C) injection were transplanted into lethally irradiated C57BL/6 congenic (CD45.1) recipients together with competitor BM cells (4×10^5) from C57BL/6 heterozygous congenic (CD45.1/CD45.2) mice.

Colony formation assay

A colony formation assay was performed as described previously (Matsumoto et al., 2011). LSK cells isolated from mice at 4 weeks after poly(I:C) injection were subjected to a colony formation assay with or without prior coculture with OP9 cells. Colony formation capacity was examined for 500 LSK cells or 200 long-term HSCs per dish with MethoCult medium. For a serial replating assay, cells from the first plating were collected and counted, and 1×10^4 of the cells were replated.

RT and real-time PCR analysis

Total RNA isolated from 3000 sorted cells with the use of Isogen and Ethachinmate was subjected to RT with a QuantiTect Reverse Transcription Kit, and the resulting cDNA was subjected to real-time PCR analysis with SYBR Green PCR Master Mix and specific primers in a StepOnePlus Real-Time PCR System (Applied Biosystems). The amounts of target mRNAs were normalized by that of Actb mRNA.

ChIP-qPCR

ChIP was performed as described previously (Artinger et al., 2013; Chapple et al., 2018). BM mononuclear cells isolated from WT mice at 14 weeks of age were fixed with 0.5% paraformaldehyde at room temperature for 10 min, after which glycine was added to a final concentration of 125 mM and the cells were incubated at room temperature for an additional 3 min. The cells were collected by centrifugation at 400 × *g* for 5 min at 4°C, washed twice with PBS, suspended in PBS supplemented with 2% heat-inactivated FBS, incubated for 30 min on ice with antibodies for the isolation of long-term HSCs, washed, and then sorted. Fixed long-term HSCs (30,000 cells) were sorted into PBS supplemented with 5% heat-inactivated FBS and collected by centrifugation at 400 × *g* for 5 min at 4°C. The BM cells or long-term HSCs were lysed in ChIP buffer [5 mM HEPES-KOH (pH 8.0), 200 mM KCl, 1 mM $CaCl_2$, 1.5 mM $MgCl_2$, 5% sucrose, 0.5% Nonidet P-40, 1 × proteinase inhibitor cocktail], and the lysate was subjected to ultrasonic treatment with a Bioruptor for 20 min (High setting for 30 s on and 30 s off) and then centrifuged at 20,000 × *g* for 20 min at 4°C. The supernatant was incubated with rotation overnight at 4°C with magnetic bead–conjugated antibodies to CHD8 (or control IgG). The bound proteins were washed with ChIP buffer for 3 times, and then eluted from the beads, cross-links were reversed by incubation overnight at 65°C with elution buffer [50 mM Tris-HCl (pH 8.0), 10 mM EDTA (pH 8.0), 1% SDS], and DNA was purified with the use of a MinElute PCR Purification Kit and subjected to real-time PCR analysis as described above.

RNA-sequencing analysis

Long-term HSCs (2×10^3 $CD48^-CD150^+$ LSK cells) from each of three mice were sorted directly into Isogen, and total RNA was purified with the use of a NucleoSpin RNA XS device and then subjected to mRNA amplification and RT with the use of a SMART-Seq v4 Ultra Low Input RNA Kit for Sequencing. Amplified cDNA was subjected to fragmentation and labeling with the use of a Nextera XT DNA Library Prep Kit, and was then sequenced with a NovaSeq 6000 system (Illumina). Paired-end reads were mapped against the mouse (mm10) genome with the use of HISAT2, and data normalization was performed with DESeq2. The expression data were analyzed with GSEA v4.1.0 software. The p53 pathway gene sets were generated from the core set of high-confidence p53 target genes (Allen et al., 2014; Fischer, 2017, 2019), and the WNT_TARGET_GENES gene set was generated from Wnt/β-catenin target genes identified in various tumors and normal tissues (Dietrich et al., 2014) (listed at https://web.stanford.edu/group/nusselab/cgi-bin/wnt/target_genes). The KEGG_WNT_SIGNALING_PATHWAY, KENNY_CTNNB1_TARGETS_UP, IVANOVA_HEMATOPOIESIS_STEM_CELL, CONRAD_STEM_CELL, and BYSTRYKH_HEMATOPOIESIS_STEM_CELL_QTL_CIS gene sets were obtained from the Molecular Signatures Database v4.0 distrubuted at the GSEA Web site.

Immunoblot analysis

Immunoblot analysis was performed as previously described (Hatakeyama et al., 2004; Takahashi et al., 2005). Long-term HSCs (1.2×10^4 cells) isolated from mice at 4 weeks after the last poly(I:C) injection were subjected to immunoblot analysis with mouse antibodies to CHD8 (generated by A. Kikuchi, Hiroshima University, Japan) and to smooth muscle actin.

Immunofluorescence staining

Immunofluorescence staining was performed as described previously (Flach et al., 2014). Long-term HSCs (2×10^3 $CD48^-CD150^+$ LSK cells) were sorted into PBS supplemented with 5% heat-inactivated FBS, seeded onto poly-L-lysine–coated slides, incubated for 10 min at room temperature, fixed with 4% paraformaldehyde for 10 min at room temperature, permeabilized with 0.15% Triton X-100 for 2 min at room temperature, and then incubated overnight at 4°C with rabbit antibodies to γ-H2AX diluted in PBS containing 1% bovine serum albumin. The cells were washed three times with PBS, incubated for 1 h at room temperature with Alexa Fluor 488–conjugated goat secondary antibodies diluted in PBS containing 1% bovine serum albumin, washed three times with PBS, and incubated for 10 min at room temperature with 4′,6-diamidino-2-phenylindole (DAPI) in PBS. After an additional three washes with PBS, the cells were mounted with Fluoromount and examined with an LSM 700 fluorescence microscope (Zeiss).

Hematologic and biochemical analyses

Hematologic and biochemical parameters were determined with the use of a Sysmex K-4500 automated hematology analyzer.

QUANTIFICATION AND STATISTICAL ANALYSIS

Quantitative data are presented as means ± SD as indicated and were compared between groups with the two-tailed Student's t test or log-rank test as performed with Microsoft Excel software or JMP Pro software. A p value of < 0.05 was considered statistically significant.